Taut foliations, positive braids, and the L-space conjecture:

Author: Siddhi Krishna

Boston College Electronic Thesis or Dissertation, 2020

Taut foliations, positive braids, and the L–space conjecture

Siddhi Krishna

A dissertation submitted to the Faculty of the
Department of Mathematics in partial fulfillment of the
requirements for the degree of Doctor of Philosophy.

Boston College
Morrissey College of Arts and Sciences
Graduate School

March 2020

Taut foliations, positive braids, and the L–space conjecture

Siddhi Krishna

Advisor: Joshua Evan Greene, Ph.D.

Abstract

We construct taut foliations in every closed 3–manifold obtained by r–framed Dehn surgery along a positive 3–braid knot K in S^3, where $r < 2g(K)-1$ and $g(K)$ denotes the Seifert genus of K. This confirms a prediction of the L–space conjecture. For instance, we produce taut foliations in every non–L–space obtained by surgery along the pretzel knot $P(-2,3,7)$, and indeed along every pretzel knot $P(-2,3,q)$, for q a positive odd integer. This is the first construction of taut foliations for every non–L–space obtained by surgery along an infinite family of hyperbolic L–space knots. We adapt our techniques to construct taut foliations in every closed 3–manifold obtained along r–framed Dehn surgery along a positive 1–bridge braid, and indeed, along any positive braid knot, in S^3, where $r < g(K) - 1$. These are the only examples of theorems producing taut foliations in surgeries along hyperbolic knots where the interval of surgery slopes is in terms of $g(K)$.

Contents

List of Figures

Acknowledgements

As I reflect upon my career thus far, I am overwhelmed with gratitude. Many people have positively impacted me professionally and personally, and I am delighted to have the opportunity to thank them for their guidance, support, and friendship.

It is a pleasure to thank my advisor Josh Greene. I have learned so much by hearing his perspective on and insights into mathematical arguments. I have always admired Josh's clarity in mathematical communication, whether in papers, the classroom, or seminar talks: I thank him for helping me develop these critical skills myself. Josh has been an amazing advocate and I am grateful for his conscientious and thoughtful advice.

Boston College has been an incredible place to be a graduate student: the community of faculty, graduate students, and postdocs is unmatched, and I have many to thank. Tao Li generously shares his time with me, answering my many questions (with multiplicity!). I am grateful that he helped me develop my topological intuition. I have enjoyed countless conversations with John Baldwin, who enthusiastically shows me the greater topological landscape, and encourages me to learn and try new things. Eli Grigsby is an incredible mentor and friend – I thank her for always believing in me, especially when I didn't believe in myself.

As a second year student, Ian Biringer organized a learning seminar, themed around the works of Bill Thurston. Ian suggested I learn about the Thurston norm – this planted the seeds for the research program I pursued for much of graduate school. I thank him for giving me direction when I didn't know where to start.

Extra special thanks to Peter Feller and Kyle Hayden, the best unofficial mathematical older brothers anyone could ever ask for! Since day one, they have generously shared their time, ideas, and insights. Chatting math with them is one of my favorite pastimes – I am grateful for their kindness and support.

Over the course of six years, Ben Howard patiently answered every question I ever asked. I thank him, Kathryn Lindsey, Mark Reeder, and David Treumann for giving me thoughtful advice every time I asked.

I enjoyed shooting the breeze with Mustafa Cengiz, Tom Cremaschi, Jonah Gaster, Spencer Leslie, Cristina Mullican, and Patrick Orson; they are wonderful colleagues, and I thank them for the fun. Sol Friedberg, Rob Meyerhoff, and Martin Bridgeman all served in the official capacities of department chair and grad chair while I was a graduate student – I thank them, as well as Marilyn Adams and Jo–Ann Bowen Coe, for keeping everything running smoothly. Boston College has been a wonderful place to be a graduate student, and I am grateful to everyone who cultivated the atmosphere.

I have greatly benefitted from the support of the low–dimensional topology community, which welcomes young students with enthusiasm. In particular, thanks to Liam Watson and Jen Hom for their encouragement over the years.

Over the years, I was lucky to have many wonderful teachers. My high school teachers Charles Petrizzi and Lisa Honeyman encouraged me to study math in college; and, once I got there, Ruth Charney persuaded me to consider graduate school. I thank them for opening my eyes to a mathematical education and career, respectively. As a graduate student, I was incredibly lucky to learn the teaching ropes from Juliana Belding, Ellen Goldstein, and Reva Kasman; they are incredible role models and mentors, showing me how to incorporate good teaching practices while developing my own style. I am grateful for their guidance, and for setting a high bar!

Reva and I met at BEAM; I thank her, Lynn Cartwright–Punnett, Cory Colbert, Dan May, and Dan Zaharopol for welcoming me to the community.

Much of my time at BC was spent thinking at my work–away–from–work, Simon's Coffee Shop. I thank everyone affiliated for making it the best place to hang out.

My friends and family have provided endless support and love over the years.

Brittney Gardner, Charlotte Kelley, Katherine Raoux have seen my highest highs and lowest lows – I thank them for making me laugh when I needed it the most. Shout out to John Bergdall and Emily Schafly, too! Thanks to my brothers, Karna, Jeetu, and Bheeshma, who always answer the phone when I call.

Finally, thanks to my parents, J.V. & Suchitra Krishna, for everything (especially the dosas). This work is dedicated to them.

Chapter 1

Introduction

1.1 A little history

Low–dimensional topology is the study of 3– and 4–manifolds, and the knots and surfaces that live inside them. To understand these spaces, topologists consider the following fundamental questions:

Question 1.1. *How do we build (interesting) 3– and 4–manifolds?*

Question 1.2. *If presented two manifolds, how could we distinguish them?*

To approach the first question, one develops constructive techniques, while the second question typically requires studying invariants associated to your objects.

In 1938, Max Dehn proposed a way to build 3–manifolds [Deh10]. **Dehn surgery** is the process of choosing a knot in a 3–manifold, removing a tubular neighborhood of it (which is homeomorphic to a solid torus), and regluing a solid torus via some homeomorphism from the boundary to that of the knot exterior; there are $\mathbb{Q}$–many ways to perform this operation. In the 1960's, Lickorish and Wallace independently proved that *every* closed, connected, oriented 3–manifold is obtained by surgery along some *link* (a collection of knots) in S^3 [Lic62, Wal60]. Thus, Dehn surgery is a powerful technique used to construct 3–manifolds, and it has become a prominent area of study within low–dimensional topology. Questions about this construction abound:

Question 1.3. *Which manifolds are obtained by surgery along* ***knots****?*

Question 1.4. *Fix a knot K. What manifolds are obtained by surgery along K?*

Question 1.5. *If $M \approx S^3_r(K)$, to what extent does M determine K? That is, if we fix a manifold M, which knots admit a surgery to M?*

Question 1.6. *If $M \approx S^3_r(K)$, to what extent does K determine M? That is, if we fix a manifold M and a surgery coefficient r, can multiple knots admit an r–framed surgery to M?*

In general, these are very difficult to answer! In fact, even the simplest versions have notorious resolutions. For example, consider perhaps the simplest instance of Question 1.5: *which knots admit a non–trivial surgery to S^3?* Using a technique known as **graphs of surface intersections**, Gordon–Luecke famously showed:

Theorem 1.7 ([GL89])**.** *If $S^3_r(K) \approx S^3$ and $r \in \mathbb{Q}$, then K is the unknot, and $r = 1/n$.*

In the direction of Question 1.6, Kronheimer–Mrowka–Ozsváth–Szabó resolved Gordon's conjecture, using **monopole Floer homology**, a powerful package of invariants:

Theorem 1.8 ([KMOS07])**.** *Let U denote the unknot in S^3, and let K be any knot. If there is an orientation-preserving diffeomorphism $S^3_r(K) \approx S^3_r(U)$, for $r \in \mathbb{Q}$, then $K \approx U$.*

Another instance of Question 1.5, known as the *Property R conjecture*, occurs when $M \approx S^1 \times S^2$. For homological reasons, the surgery coefficient must be 0, reducing the question to: *when is* 0*–surgery along a knot* $S^1 \times S^2$? In his seminal work, Gabai proved:

Theorem 1.9 ([Gab87])**.** *The only knot admitting a* 0*–surgery to* $S^1 \times S^2$ *is the unknot.*

Gabai's proof uses **taut foliations**: A ***foliation*** of a 3–manifold Y is a decomposition into (typically non–compact) surfaces, called ***leaves***. A foliation is ***taut*** if there exists a simple closed curve meeting each leaf transversely. That is, we try to study a 3–manifold by understanding if and how it can be decomposed into simpler (2–dimensional) pieces.

Though every 3–manifold admits a foliation, not all of them admit *taut* ones! For instance, in his thesis, Reeb showed that S^3 cannot be tautly foliated [Ree52]. In his proof, he constructed the so–called **Reeb foliation** of a solid torus. A foliation without a **Reeb component** is called **Reebless**. We note that if a foliation is taut, then it is Reebless; the converse is not true.

Later, Novikov showed that if M^3 has a taut foliation, then the fundamental group is infinite [Nov65]; indeed, the closed transversal has infinite order in $\pi_1(M)$. Therefore, elliptic manifolds (i.e. those obtained as a quotient of S^3) cannot be tautly foliated.

For a time, taut foliations were used to investigate Thurston's geometrization conjecture: Thurston proved that if K is a hyperbolic knot in S^3, then all but finitely many manifolds obtained by Dehn surgery along K are hyperbolic [Thu97] (this can be interpreted as one geometric approach to Question 1.4). It was conjectured that every hyperbolic 3–manifold had a Reebless foliation, and this could serve as an approach to Thurston's geometrization. This line of inquiry was vanquished by Roberts–Shareshian–Stein, who showed that there exist infinitely many hyperbolic 3–manifolds not admitting Reebless foliations [RSS03].

Nevertheless, an expectation persisted: in some appropriate sense, "most" hyperbolic 3–manifolds should admit taut foliations. A good recalibration requires *Heegaard Floer homology.* First introduced by Ozsváth–Szabó in the early 2000s, this powerful package of invariants has been instrumental in answering long–standing questions in geometric topology (especially questions about Dehn surgery). The Heegaard Floer homology of a 3–manifold Y is an algebraic invariant, computed using analytic data. In this context, there is a natural notion of a "smal" 3–manifold, from the Floer–homological perspective:

Definition 1.10. *An irreducible rational homology 3–sphere Y is an* ***L–space*** *if it is small from the perspective of Heegaard Floer homology: that is, equality is obtained in rank$(\widehat{HF}(Y;\mathbb{Z}/2\mathbb{Z})) \geq |H_1(Y;\mathbb{Z})|$.*

Lens spaces and elliptic manifolds are prominent examples of L–spaces. A standard technique to build L–spaces is via Dehn surgery:

Definition 1.11. *A knot $K \subset S^3$ is an* ***L–space knot*** *if there exists some $r > 0$ such that $S^3_r(K)$ is an L–space.*

Tours knots [Mos71] and the Berge knots [Ber18] admit lens space surgeries, so they are L–space knots. In fact, if a knot admits a surgery to a single L–space, it admits infinitely many:

Theorem 1.12 ([KMOS07, RR17])**.** *Suppose a non–trivial knot $K \subset S^3$ is an L–space knot. Then for all $r \geq 2g(K) - 1, S^3_r(K)$ is an L–space.*

Ozsváth–Szabó showed that L–spaces cannot admit taut foliations [OS05]. This theorem, combined with Thurston's hyperbolic Dehn surgery result, presents a Floer–homological counterpoint to the result of Roberts–Shareshian–Stein: let K be a hyperbolic L–space knot, and consider the collection of manifolds obtained by r–framed Dehn surgery along K, where $r \geq 2g(K) - 1$. All but finitely many of these manifolds are hyperbolic, yet none can admit taut foliations! This leads to the following natural question:

Question 1.13. *In what ways is the* ***geometric*** *notion of a taut foliation related to the* ***Floer–homological*** *notion of an L–space?*

Investigating this question sparked many new avenues within the low–dimensional topology community, culminating in a unexpected conjecture.

1.2 Modern motivation and summary of results

The L-space Conjecture predicts a surprising relationship between Floer-homological, algebraic, and geometric properties of a closed 3-manifold Y:

Conjecture 1.14 (The L-space Conjecture [BGW13, Juh15])**.** *Suppose Y is an irreducible rational homology 3-sphere. Then the following are equivalent:*

1. *Y is a non-L-space (i.e. the Heegaard Floer homology of Y is not "simple"),*
2. *$\pi_1(Y)$ is left-orderable, and*
3. *Y admits a taut foliation.*

Work by many researchers fully resolves Conjecture 1.14 in the affirmative for graph manifolds [BC15, BC17, BGW13, BNR97, CLW13, EHN81, HRRW15, LS09]. Combining results of Ozsváth-Szabó, Bowden, and Kazez-Roberts proves that if Y admits a taut foliation, then Y is a non-L-space [OS04, Bow16, KR17]. Here, we investigate the converse.

One strategy for producing non-L-spaces is via Dehn surgery. A non-trivial knot $K \subset S^3$ is an **L-space knot** if *some* non-trivial surgery along K produces an L-space. Lens spaces are prominent examples of L-spaces, so any knot with a non-trivial surgery to a lens space (notably Berge knots [Ber18]) is an L-space knot. Berge-Gabai knots are the subclass of 1-bridge braids in S^3 admitting lens space surgeries [Gab90, Ber18], yet *every* 1-bridge braid is an L-space knot [GLV18].

In fact, if K is an L-space knot, *infinitely* many surgeries along K yield L-spaces. In particular, for any K realized as the closure of a positive braid, the set of L-space surgery slopes is either $[2g(K)-1,\infty)\cap\mathbb{Q}$, or the empty set [Liv04, OS05, KMOS07, RR17]. Thus, r-framed Dehn surgery along *any* non-trivial knot realized as a positive braid closure yields a non-L-space for all $r < 2g(K)-1$. This viewpoint guides our treatment of Conjecture 1.14, which predicts these manifolds admit taut foliations.

Theorem 1.15. *Let K be a knot in S^3, realized as the closure of a positive 3-braid. Then for every $r < 2g(K) - 1$, the knot exterior $X_K := S^3 - \mathring{\nu}(K)$ admits taut foliations meeting the boundary torus T in parallel simple closed curves of slope r. Hence the manifold obtained by r-framed Dehn filling, $S^3_r(K)$, admits a taut foliation.*

Remark 1.16. *Theorem 1.15 can be reformulated as follows: for K and r as above, the manifold $S^3_r(K)$ admits a taut foliation, such that the core of the Dehn surgery is a closed transversal.*

A 3-stranded twisted torus knot is a knot obtained as the closure of $(\sigma_1\, \sigma_2)^q(\sigma_2)^{2s}$, where q and s are positive integers, and σ_1, σ_2 are the standard Artin generators. Vafaee proved every 3-stranded twisted torus knot is an L-space knot [Vaf15]. Moreover, if an L-space knot admits a presentation as a 3-braid closure, then K is a twisted torus knot [LV19]. Thus, hyperbolic L-space knots are abundant among positive 3-braid closures. Applying Theorem 1.15 yields:

Corollary 1.17. *In Conjecture 1.14, (1) $\iff$ (3) holds for all Dehn surgeries along an infinite family of hyperbolic L-space knots.* □

Baker-Moore, strengthening results of Lidman-Moore, proved that the only L-space Montesinos knots are the pretzel knots $P(-2, 3, q)$, for $q \geq 1$, q odd [LM16, BM18]. These knots are realized as closures of positive 3-braids (see Figure 10). Applying Theorem 1.15, we deduce:

Corollary 1.18. *Let K be an L-space Montesinos knot in S^3. Then for any r-framed surgery on K, the surgered manifold $Y = S^3_r(K)$ is a non-L-space $\iff$ Y admits a taut foliation.* □

We note that Delman-Roberts recover Corollary 1.18 in forthcoming work [DRb].

The Fintushel-Stern pretzel knot $P(-2, 3, 7)$ is a hyperbolic knot in S^3 admitting lens space surgeries [FS80], hence is an L-space knot. It can be realized as a positive 3-

braid closure in S^3 (see Figure 10). In Section 3.2, we explicitly construct the family of taut foliations meeting the boundary torus T in all rational slopes $r < 2g(K)-1 = 9$.

Tran, generalizing work of Nie [Nie19], showed that for any K in an infinite subfamily $\mathcal{F}$ of 3-stranded twisted torus knots, and $r \geq 2g(K) - 1$, $\pi_1(S^3_r(K))$ is not left-orderable [Tra19]. The L-space pretzel knots comprise a proper subset of $\mathcal{F}$. We conclude:

Corollary 1.19. *Suppose Y is obtained by r-framed Dehn surgery along K in S^3, for K a 3-stranded twisted torus knot in $\mathcal{F}$, and $r \in \mathbb{Q}$. Then*

$$\pi_1(Y) \textit{ is not left-orderable} \impliedby Y \textit{ is an L-space} \iff Y \textit{ does not admit a taut foliation.}$$

That is, (2) $\implies$ (1) $\iff$ (3) of Conjecture 1.14 holds for manifolds obtained by Dehn surgeries along knots in $\mathcal{F}$.

Our methods for proving Theorem 1.15 are constructive. Inspired by work of Roberts [Rob01a, Rob01b], we build **sink disk free** branched surfaces in fibered knot exteriors. By Li [Li02, Li03], these branched surfaces carry essential laminations. We first extend these laminations to taut foliations in knot exteriors, and then to taut foliations in surgered manifolds.

Conjecture 1.14 predicts Theorem 1.15 holds for any knot K realized as a positive braid closure, on any number of strands. Any such K is fibered; applying [Rob01b], $S^3_r(K)$ admits a taut foliation for any $r < 1$. An

In Chapter 4, we prove adapt of our techniques to partially close the gap between Roberts' result and the prediction for 1-bridge braids in S^3:

Theorem 1.20. *Let K be any (positive) 1-bridge braid in S^3, i.e. K is a knot in S^3, realized as the closure of a braid β on w strands, where*

$$\beta = (\sigma_b \sigma_{b-1} \ldots \sigma_2 \sigma_1)(\sigma_{w-1}\sigma_{w-2} \ldots \sigma_2 \sigma_1)^t$$

for $w \geq 3, 1 \leq b \leq w-2, t \geq 1$. Then for every $r < g(K)$, the knot exterior $X_K := S^3 - \mathring{\nu}(K)$ admits taut foliations meeting the boundary torus T in parallel simple closed curves of slope r. Hence the manifold obtained by r-framed Dehn filling, $S^3_r(K)$, admits a taut foliation.

This serves as a warm–up for Theorem 1.21 below; we further modify our techniques to leverage some hidden flexibility in both our construction and positive braids.

Theorem 1.21. *Suppose K is a knot in S^3 which can be realized as the closure of a positive braid on n strands. Then for all $r \in (\infty, g(K)-1)$, $S^3_r(K)$ admits a taut foliation.*

Remark 1.22. *To prove Theorem 1.21, we will divide the set of all positive n–braids with prime closure into four categories, based on the parity of the braid index. Our proof shows that we can construct taut foliations in $S^3_r(K)$ for all $r \in (-\infty, g(K))$ for three of the four categories.*

This is proved in Chapter 5.

Remark 1.23. *These are the **only** examples in the literature of theorems producing taut foliations in surgeries along hyperbolic knots where the interval of surgery slopes is in terms of $g(K)$.*

1.3 Why positive braids?

Throughout this work, we focus on the class of *positive braid knots* – the knots in S^3 which can be realized as the closure of a positive braid. Why these knots in particular?

As indicated in Sections 1.1 and 1.2, L–space knots are special from the Dehn surgery perspective, as they admit surgeries to the simplest 3–manifolds, L–spaces. Thus far, a classification of L–space knots remains elusive, and there are few examples in the literature of such knots [Mos71, Ber18, GLV18]. However, it is known that L–space knots are **fibered** [Ghi08, Ni07]: the knot exterior has the structure of a surface bundle over a circle, as below. Here, F is a compact, connected, oriented surface with a single boundary component.

$$X_K := S^3 - \mathring{\nu}(K) = (F \times I) \Big/ (x,1) \sim (\varphi(x), 0)$$

Thus, if we would like to probe the L–space conjecture *and* investigate a potential classification of L–space knots, the following is a good place to start:

Goal: *Build taut foliations in manifolds obtained by Dehn surgery along fibered knots.*

One way to study a fibered knot is to focus on the associated **monodromy**, i.e. the (conjugacy class of the) diffeomorphism used to build the mapping torus. Honda–Kazez–Matíc showed that these diffeomorphisms can be sorted into three categories, based on the **fractional Dehn twist coefficient** (FDTC), which (morally speaking) measures how much the diffeomorphism "twists about the boundary" [HKM07] (see [KR13] for a nice summary):

- $FDTC(K) > 0$ (i.e φ is *right–veering*)
- $FDTC(K) < 0$ (i.e φ is *left–veering*)
- $FDTC(K) = 0$ (i.e. φ is *neither right– nor left–veering*)

Rather than venture into a discussion on veering–ness here, we focus on some applications and consequences of their theorem. Roberts proved that if K is a hyperbolic fibered knot in S^3 with $FDTC(K) = 0$, then for every $r \in \mathbb{Q}$, $S^3_r(K)$ has a taut foliation [Rob01b]. So, to pursue our stated goal, we need only consider the first two cases.

Moreover, if a fibered knot K has right–veering monodromy, then the mirror $m(K)$ has left–veering monodromy: so, we restrict our attention to the former. Indeed, if a knot admits a *positive* surgery to an L–space, it must have right–veering monodromy [Hed10].

In fact, Hedden showed that L–space knots are **strongly quasi–positive** (SQP): they are realized as closures of strongly quasi–positive braids [Hed10]. These braids have rigid braid word presentations: define

$$\sigma_{i,j} := (\sigma_i \sigma_{i-1} \dots \sigma_{j-2})(\sigma_{j-1})(\sigma_i \sigma_{i-1} \dots \sigma_{j-2})^{-1}$$

A braid β is **strongly quasi–positive** if

$$\beta = \prod_{k=1}^{m} \sigma_{i_k, j_k}$$

Therefore, to probe Conjecture 1.14, we amend our goal:

Goal (redux): *Build taut foliations in manifolds obtained by Dehn surgery along fibered, strongly quasi–positive knots.*

It is reasonable to expect that the data of the monodromy be used explicitly, in some capacity. There is a minor hiccup to this approach – in general, it can be difficult to identify the monodromy of a fibered SQP knot! However, we observe that *positive* braid knots are examples of fibered SQP knots where we *can* identify a concrete factorization of the monodromy (see Sections 2.2 and 2.3).

Thus, positive braid knots serve as an ideal testing ground for investigating Conjecture 1.14 and the Goal (redux). This informs our perspective for this body of work.

1.4 Organization

In Chapter 2, we present the necessary background on branched surfaces, fibered knot detection and product disks, and positive braid closures as Hopf plumbings.

In Chapter 3, we first establish the foundations for proving Theorem 1.15. Along the way, we construct taut foliations for every $S^3_r(K)$, where $K = P(-2,3,7)$ and $r < 9$. In particular, this constructs taut foliations in every non–L–space obtained by surgery for this knot. Afterwards, we prove Theorem 1.15.

In Chapter 4, we consider 1-bridge braids, and construct taut foliations in $S^3_r(K)$ where $r \in (-\infty, g(K))$. This proves Theorem 1.20, and prepares us for Chapter 5.

In Chapter 5, we construct taut foliations in $S^3_r(K)$, where $r \in (\infty, g(K) - 1)$ and K is any (prime) positive braid knot. This proves Theorem 1.21.

In Chapter 6, we present some concluding remarks and future directions.

1.5 Conventions

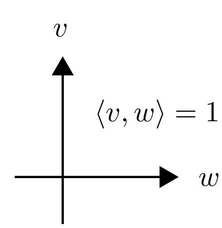

- We work only with braid closures which are knots in S^3.
- For any knot exterior X_K, $H_1(\partial X_K)$ is generated by the Seifert longitude λ and the standard meridian μ.
- Let $\langle \alpha, \beta \rangle$ denote the algebraic intersection number; following the sign convention above, we set $\langle \lambda, \mu \rangle = 1$. For any essential simple closed curve γ on $T = \partial X_K$, the slope of γ is determined by $\dfrac{\langle \gamma, \lambda \rangle}{\langle \mu, \gamma \rangle}$.
- We use $\sigma_1, \sigma_2, \ldots, \sigma_{n-1}$ to represent the standard Artin generators for the n-stranded braid group. Strands are drawn vertically, oriented “down", and enu-

merated from left-to-right. Given a braid diagram, we recover the braid word by reading β from top-to-bottom.

- The surface F will always be orientable; in all figures of Seifert surfaces, only F^+ is visible.

- If a properly embedded arc α lies on F^-, it is drawn with a blue dotted line; if α lies on F^+, it is drawn with a pink solid line. A helpful mnemonic: "**p**ink" and "**p**lus" both start with "**p**".

- Given a fibered knot $K \subset S^3$ with fiber F and monodromy φ, the knot exterior is a mapping torus $F \times [0,1]/\sim$, where $(x,0) \sim (\varphi(x),1)$. Moreover, $\varphi \approx \mathbb{1}$ in $\nu(\partial F)$.

Chapter 2

Background

2.1 Branched Surfaces

Our primary tool for constructing taut foliations are branched surfaces. For a detailed exposition on branched surfaces, see Floyd-Oertel [FO84].

Definition 2.1. *A* ***spine for a branched surface*** *is a 2-complex in a 3-manifold M, locally modeled by:*

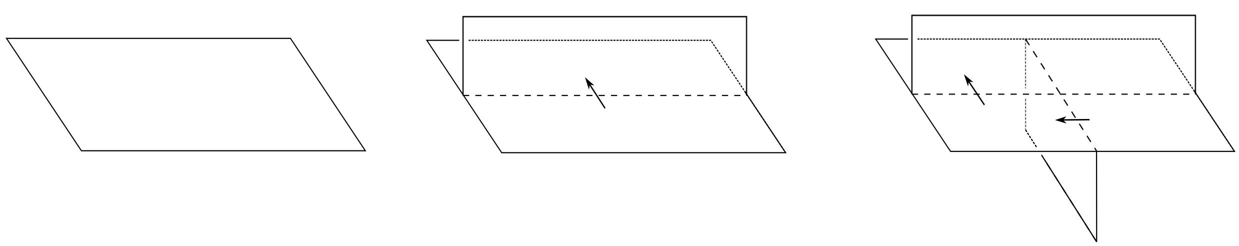

Figure 1: Ignoring the arrows yields the local models for the spine of a branched surface.

Definition 2.2. *A* ***branched surface*** *B in a 3-manifold M is built by providing smoothing/cusping instructions for a spine. It is locally modeled by:*

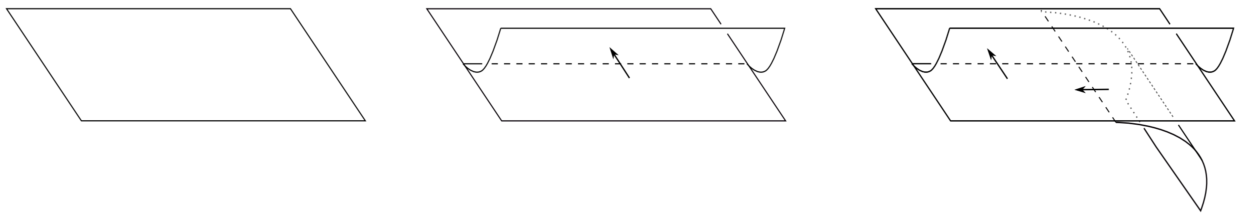

Figure 2: The cusping instructions for the spine in Figure 1 yield these local models.

A branched surface is locally homeomorphic to a surface everywhere except in a set of properly embedded arcs and simple closed curves, called the **branch locus** γ. A point p in γ is called a **triple point** if a neighborhood of p in B is locally modeled by the rightmost picture of Figure 2. A **branch sector** is a connected component of $\overline{B-\gamma}$ (the closure under the path metric). In this paper, all branched surfaces meet the boundary torus of X_K; it will do so in a train track.

Definition 2.3. *A **sink disk** [Li02] is a branch sector S of B such that (1) S is homeomorphic to a disk, (2) $\partial S \cap \partial M = \varnothing$, and (3) the branch direction of every smooth arc or curve in its boundary points into the disk. A **half sink disk** [Li03] is a branch sector S of B such that (1) S is homeomorphic to a disk, and (2) $\partial S \cap \partial M \neq \varnothing$, and (3) the branch direction of each arc in $\partial S - \partial M$ points into S. Note: $\partial S \cap \partial M$ may not be connected. When a branched surface B contains no sink disk or half sink disk, we say B is **sink disk free**. See Figure 3.*

Thus, to prove a branched surface is sink disk free, we need only check that some cusped arc points out of each branch sector. Indeed, this is the heart of the proof of Theorem 1.15.

Gabai and Oertel prove a lamination $\mathcal{L}$ is essential if and only if $\mathcal{L}$ is carried by an essential branched surface B [GO89]. Li proves that for B to carry an essential lamination, it suffices to be sink disk free:

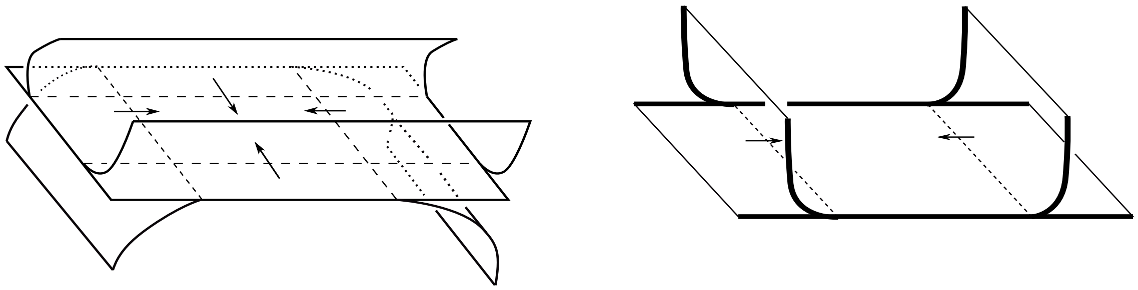

Figure 3: On the left, the local model of a **sink disk**. On the right, the **bolded** lines lie on $\partial M \approx T^2$; this is the local model for a **half sink disk**.

Theorem 2.4 (Theorem 2.5 in [Li03])**.** *Suppose M is an irreducible and orientable 3-manifold whose boundary is an incompressible torus, and B is a properly embedded branched surface in M such that*

(1a) $\partial_h(N(B))$ is incompressible and ∂-incompressible in $M - int(N(B))$

(1b) There is no monogon in $M - int(N(B))$

(1c) No component of $\partial_h N(B)$ is a sphere or a disk properly embedded in M

(2) $M - int(N(B))$ is irreducible and $\partial M - int(N(B))$ is incompressible in $M - int(N(B))$

(3) B contains no Reeb branched surface (see [GO89] for more details)

(4) B is sink disk free

Suppose r is any slope in $\mathbb{Q} \cup \{\infty\}$ realized by the boundary train track $\tau_B = B \cap \partial X_K$. If B does not carry a torus that bounds a solid torus in $M(r)$, the manifold obtained by r-framed Dehn filling, then (1) B carries an essential lamination in M meeting the boundary torus in parallel simple closed curves of slope r, and (2) $M(r)$ contains an essential lamination.

Remark 2.5. *Our version of Theorem 2.4 differs mildly from the version in [Li03]. The discrepancy arises from our consideration of the lamination in M; this is not* *problematic, as the lamination in $M(r)$ meets the surgery torus in simple closed curves of slope r.*

A branched surface satisfying conditions (1–4) in Theorem 2.4 is called a **laminar branched surface**. To prove Theorem 1.15 for any positive 3-braid knot K, we construct a laminar branched surface B and prove the boundary train track τ carries all rational slopes $r < 2g(K) - 1$. Applying Theorem 2.4, we deduce the existence of essential laminations in X_K, which we extend to taut foliations in X_K.

2.2 Fibered knots and product disks

Positive braid closures are fibered links [Sta78]. This statement can be proved concretely via disk decomposition [Gab86]. We recount the relevant details of Gabai's method.

For $K \subset S^3$, let F be a genus g orientable Seifert surface for K. $F \times I$ is a genus $2g$ handlebody H, and $\partial H \approx F^+ \cup F^- \cup A$, where $A \approx K \times I$. This is an example of a **sutured manifold** with annular suture A, formally written as $(F \times I, \partial F \times I) \approx (F \times I, K \times I) \approx (M, \gamma)$.

A **product disk** is a disk D^2 in the **complementary sutured manifold** $(X_F, \partial F \times I)$, $X_F := \overline{S^3 - (F \times I)}$, such that $\partial D^2 \approx S^1$ meets the suture A exactly twice. Given a product disk in X_F, we can **decompose along it**, by cutting X_F along D and creating a new sutured manifold $M' \approx \overline{X_F - (D \times I)}$. The sutures γ of M can be modified in one of two ways to form the sutures γ' of M': at the sites where $\gamma \cap \partial M'$, connect the ends of $\gamma \cap (\partial D \times (\pm 1))$ by diameters of $D \times \{\pm 1\}$. Writing $(M, \gamma) \overset{D}{\rightsquigarrow} (M', \gamma')$ denotes a **(product) disk decomposition**.

Theorem 2.6 (Theorem 1.9 in [Gab86])**.** *A link $L \subset S^3$ is fibered with fiber surface F if and only if a sequence of product disk decompositions, applied to $(X_F, \partial F \times I)$, terminates with a collection of product sutured balls $(B^3, S^1 \times I)$.*

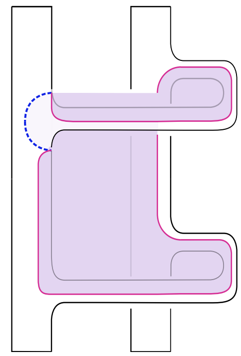

Figure 4: The product disk D for a positive Hopf Band. We see $\partial D|_{F^+ \cup F^-} \approx \alpha \cup \varphi(\alpha)$, where φ is a positive Dehn twist about the core curve.

When K is a fibered knot in S^3, the sequence of product disk decompositions terminates with a single $(B^3, S^1 \times I)$.

A sequence of disk decompositions to a product sutured ball not only certifies fiberedness, but also determines where the monodromy sends properly embedded arcs on F. Let F be a fiber surface for $K \subset S^3$; thus, $(F \times I, A)$ is a trivial product sutured manifold. Heuristically, all the data pertaining to the monodromy of the fibered knot is captured by the complementary sutured manifold. In particular, let α be an essential properly embedded arc on F^-. Now, view α as an arc on $F^- \subset \partial(F \times I)$ with $\partial\alpha \subset \partial A$. Pushing α through the complementary sutured manifold $(X_F \approx F \times I, \partial F \times I)$ yields a disk $D \approx \alpha \times I$, where ∂D meets the suture twice, and $\overline{\partial D - A} = \alpha^+ \sqcup \alpha^-$, with $\alpha^\star \subset F^\star$. D is a product disk, and $\varphi(\alpha^-) \approx \alpha^+$. See Figure 4 for an example.

Remark 2.7. *Positive braid closures are obtained by a sequence of plumbings of positive Hopf bands. One can inductively apply Corollary 1.4 in [Gab85] to produce an explicit factorization of the monodromy in terms of Dehn twists. We demonstrate this procedure alongside an example in Section 2.3.*

2.3 Positive braids and Hopf plumbings

In this section, we present an algorithm realizing the fiber surface for a positive braid knot as the plumbing of positive Hopf bands. We demonstrate the construction alongside the β below, which has braid index five:

$$\beta \approx \sigma_1\sigma_3\sigma_2\sigma_3\sigma_4\sigma_1^2\sigma_3\sigma_2\sigma_3\sigma_4\sigma_3 \tag{2.1}$$

For β a positive braid on n strands, we built F by attaching positively twisted bands to n disks, in accordance to the braid word.

Definition 2.8. *The disks used to build F are called **Seifert disks**, and we denote them as S_i, for $1 \leq i \leq n$.*

Lemma 2.9. *Let β be a positive braid on n strands. The standard Bennequin surface F, obtained by attaching positively twisted bands between n disks, is a fiber surface for $\widehat{\beta}$. Moreover, the braid word determines a factorization of the monodromy of F.*

Proof. This lemma is well known to experts; for a survey on constructing fibered knots, see [Sta78]. However, our goal is to explicitly read off the monodromy of the fibration from the braid word – accordingly, we explain the proof via an example, which illustrates how to find an explicit factorization of the monodromy.

We recall: a positive Hopf band is a fibered link in S^3; the fiber surface is an annulus, and the monodromy φ is a positive Dehn twist about the core curve c. Let H_1 and H_2 denote two positive Hopf links, with monodromies φ_1 and φ_2 respectively. Applying [Sta78], plumbing H_2 onto H_1 yields a new fibered link; as explained in [Gab85], the monodromy φ of the result is obtained via precomposition: that is, $\varphi \approx \varphi_1 \circ \varphi_2$. Now consider a sequence of plumbings of Hopf links $H_1, \ldots, H_k$ (where H_i is plumbed onto H_{i-1}). The result is a fibered link L with monodromy $\varphi = \varphi_1 \circ \ldots \circ \varphi_k$, where φ_i is a positive Dehn twist about the core curve of H_i.

This algorithm can be neatly realized in the positive braid setting: indeed, a plumbing sequence can be read off directly from the braid word. We demonstrate this procedure for the braid β in (2.1).

Definition 2.10. *Let c_i denote the total number of occurrences of σ_i in β.*

Definition 2.11. *The i^{th}* ***column of*** *F, denoted Γ_i, is the union of the Seifert disks S_i, S_{i+1}, and the bands ${}_1, \ldots {}_{c_i}$ connecting them.*

We will build the fiber surface F in stages, one column at a time. That is, we first build the surface F_1, corresponding to the first column. We iteratively build the surface F_i from F_{i-1} by first stabilizing, and then plumbing Hopf bands in accordance to the relative positions of the σ_i's with respect to the σ_{i-1}'s.

Step 0: Build the unknot as a braid closure.

Build a surface by attaching a single positively twisted band between two disks, as in the leftmost part of Figure 5. This presents the unknot as the closure on the braid $\sigma_1 \in \mathcal{B}_2$ (the braid group on two strands).

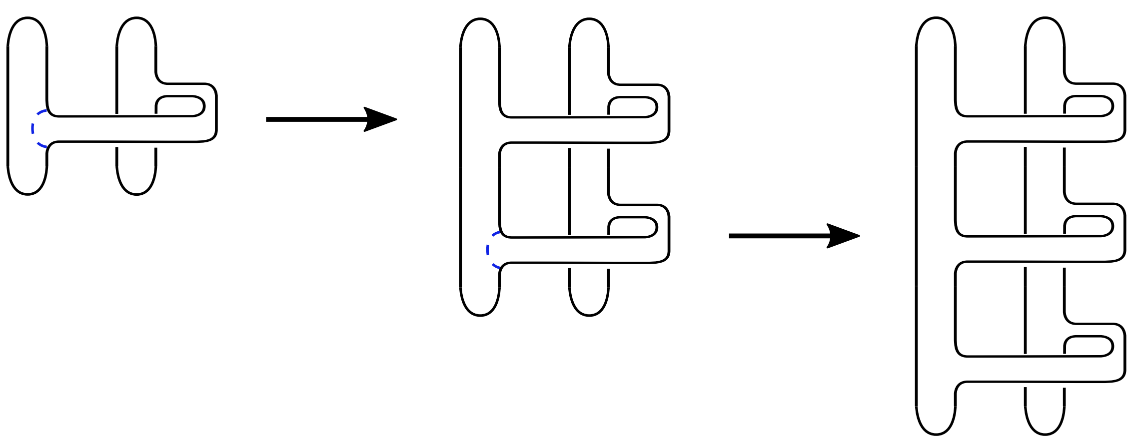

Figure 5: We build F_1 by plumbing two positive Hopf bands to the unknot. The plumbing arcs are indicated in blue.

Step 1: Build F_1.

We now build the first column of the fiber surface F: let c_1 denote the number of occurrences of σ_1 in β. Build the torus link $T(2, c_1)$ by iteratively plumbing together $c_1 - 1$ Hopf bands. Call the surface built at this stage F_1. For the braid β in (2.1), $c_1 = 3$, so we plumb 2 Hopf bands to produce $T(2, 3)$; see Figure 5.

Step 2: Build F_2 by plumbing Hopf bands to F_1.

Next, stabilize F_1, such that the stabilization occurs at the site of the first σ_2 in β, as in Figure 6 (left to middle). Note that after (possibly) conjugating, we may assume that β begins with a σ_1, so the first σ_2 in β occurs after some number of σ_1s.

The stabilization allows us to realize the same fiber surface F_1, but it is appears as the Bennequin surface of a braid on three (rather than two) strands. To build F_2, sequentially plumb $c_2 - 1$ Hopf bands, where all the plumbing arcs lie in the Seifert disk S_2. To do this, we need to identify an arc $\alpha \subset S_2$ to plumb onto.

We already identified the first occurrence of σ_2 in β (this determined the site of the stabilization). Now, identify the second occurrence of σ_2: it will occur after t occurrences of σ_1 (note that t can be zero). Let u_α and ℓ_α denote the upper and lower endpoints of the forthcoming α; both will lie on ∂S_2. Then u_α will lie above the attachment sites of the previous σ_2 band, and the ℓ_α will lie after the t right attachment sites of the σ_1 bands (if $t = 0$, then α will be isotopic to the co–core of the existing σ_2 band). Connecting u_α and ℓ_α via a simple arc in S_2 yields the plumbing arc α. That is: the plumbing arc α will "enclose" the right attachments sites of the t σ_1 bands that occur between the previous and current σ_2's in β. Repeating this process until we have exhausted all occurrences of σ_2 in β yields the fiber surface F_2.

In our example, $c_2 = 2$, and the first σ_2 occurs between the first two σ_1's, while the second σ_2 occurs after the last σ_1. Thus, we need only plumb on a single Hopf band along the arc indicated to build the surface F_2. The plumbing arc, and the

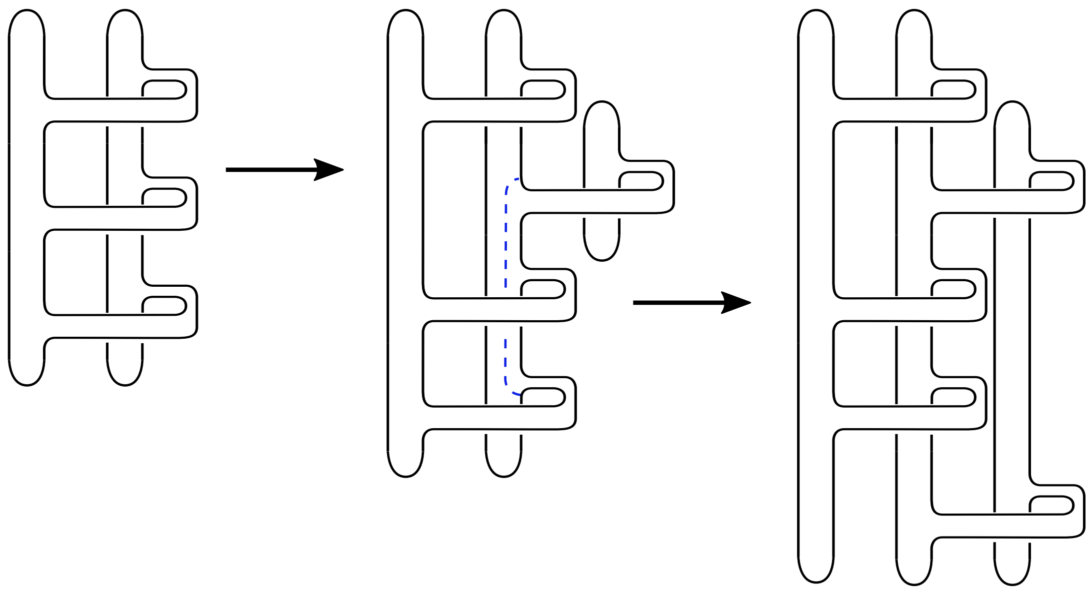

Figure 6: We build F_2 by first stabilzing F_1 (as in the middle figure), and then plumbing a single positive Hopf band along the indicated (blue) plumbing arc. The resulting surface F_2, is on the right.

result of the plumbing, are seen in Figure 6 (middle and right).

Step 3: Exhaust all σ_i's in β to build F.

We repeat this procedure to build the surface F_i, by plumbing positive Hopf bands onto F_{i-1}: for each $3 \leq i \leq n-1$, stabilize the surface F_{i-1} such that the stabilization occurs at the location of the first occurrence of σ_i in β. Then, count the number of σ_i's in β, and plumb $c_i - 1$ Hopf bands onto the stabilized F_{i-1}, while keeping track of the relative positions to the σ_{i-1}'s, as in the previous paragraph. The result is called F_i. Indeed, the surface F_{n-1} is F, the fiber surface for β. See Figures 7 and 8 to see the remainder of this procedure for β as in (2.1).

This procedure allows us to read off an explicit sequence of plumbings from the braid word. Moreover, each pair of consecutive bands between adjacent Seifert disks

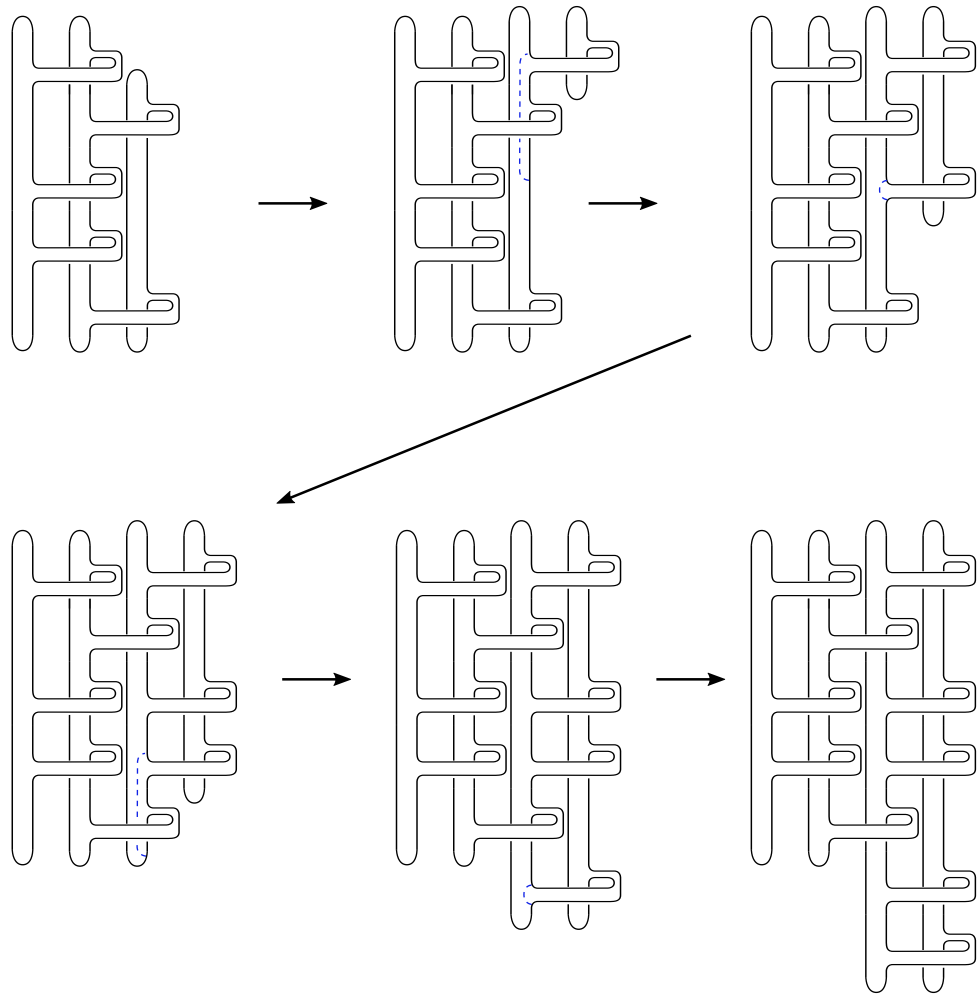

Figure 7: Building F_3 for the braid β in (2.1).

specifies a simple closed curve γ, and the monodromy of the braid will be a sequence of positive Dehn twists about the simple closed curves from the plumbings: from "bottom–to–top", we Dehn twist about the simple closed curves in Γ_{n-1}, then Γ_{n-2}, then Γ_{n_3}, until we reach the first column Γ_1. Thus, the positive braid word β not only specifies a fiber surface for $\widehat{\beta}$, but also produces an explicit factorization of the monodromy. $\square$

Remark 2.12. *This procedure also works for alternating – or more generally, homogeneous – braids. For braids of these forms, the plumbing involves both positive and negative Hopf bands, in accordance with the sign of the* σ_i *in* β*.*

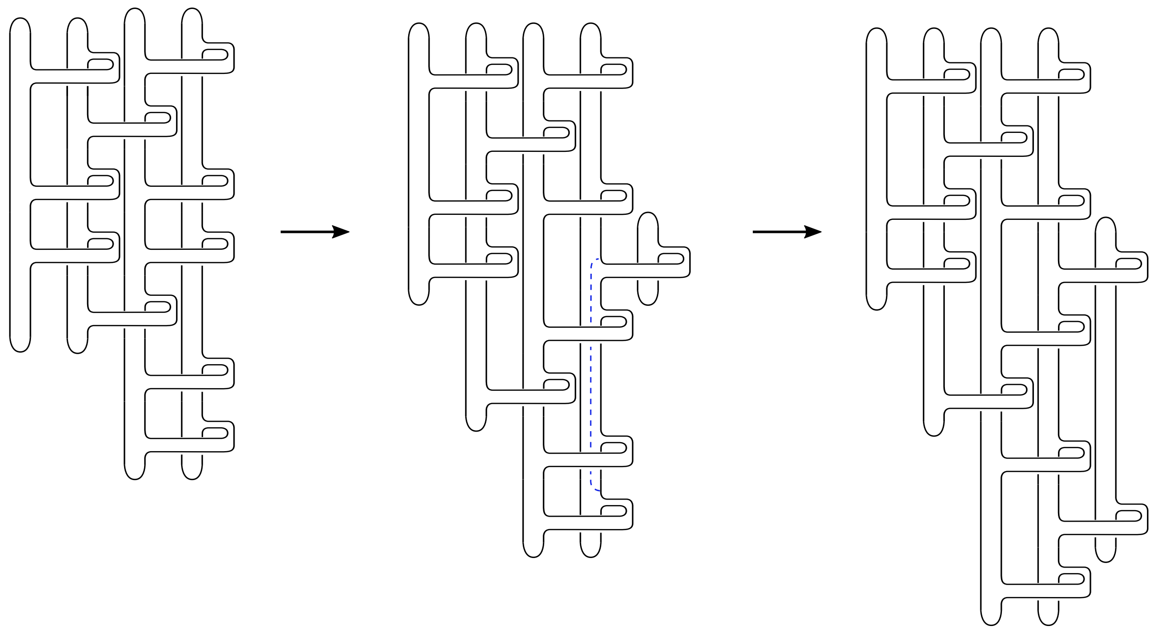

Figure 8: Building $F_4 \approx F$ for the braid β in (2.1).

Chapter 3

Positive 3–braids

3.1 Fiber surfaces for positive 3–braid closures

Let β be a positive 3-braid, where β is not one of σ_1^s, σ_2^s, or $\sigma_1\sigma_2$. For such braids, conjugation and repeated applications of the braid relation $\sigma_2\sigma_1\sigma_2 = \sigma_1\sigma_2\sigma_1$ eliminate isolated instances of σ_1 [Baa13]. Thus, every such positive 3-braid can be written in the form

$$\beta = \sigma_1^{a_1}\sigma_2^{b_1}\sigma_1^{a_2}\sigma_2^{b_2}\dots\sigma_1^{a_k}\sigma_2^{b_k}, \qquad \text{where for all } i \leq k,\ 2 \leq a_i \text{ and } 1 \leq b_i \tag{3.1}$$

Going forward, we assume all 3-braids are in this form.

Definition 3.1. *Let β be of the form described in (3.1). β has k* ***blocks****, where the i^{th} block has the form $\sigma_1^{a_i}\sigma_2^{b_i}$.*

Definition 3.2. *Let $\hat{\beta}$ denote the closure of β, which is in the form specified by Equation 3.1. Define:*

$$c_1 := \sum_{i=1}^{k} a_i \qquad\qquad c_2 := \sum_{i=1}^{k} b_i$$

Applying Seifert's algorithm to $\hat{\beta}$ yields Seifert disks S_1, S_2, S_3. Reading β from left to right, each occurrence of σ_i dictates the attachment of a positively twisted band between S_i and S_{i+1}.

Definition 3.3. *For the j^{th} letter σ_i in the braid word β, denote the corresponding positively twisted band attached between S_i and S_{i+1} as $\mathbb{b}_j$.*

The bands are attached from top to bottom; there are $c_1 + c_2$ bands attached in total. This is our fiber surface F for $\hat{\beta}$. Following conventions established by Rudolph [Rud93], we only see F^+, the “positive side" of F, in our figures.

Definition 3.4. *The bands $\mathbb{b}_j$ and $\mathbb{b}_k$ are **of the same type** if they are both attached between the Seifert disks S_i and S_{i+1}.*

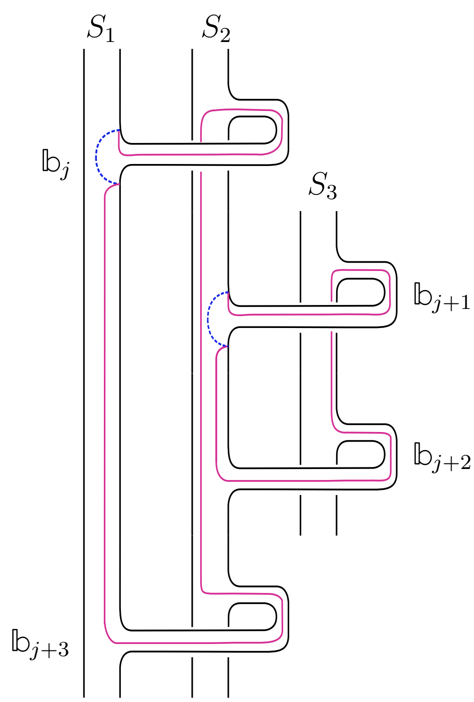

Figure 9: There are two product disks dentified, D_j and D_{j+1}. We have $\partial D_j \subset S_1 \cup S_2 \cup \mathbb{b}_j \cup \mathbb{b}_{j+3}$, and $\partial D_{j+1} \subset S_2 \cup S_3 \cup \mathbb{b}_{j+1} \cup \mathbb{b}_{j+2}$. The non-sutured portions of ∂D_j and ∂D_{j+1} are $\alpha_j^- \cup \alpha_j^+$ and $\alpha_{j+1}^- \cup \alpha_{j+1}^+$, respectively.

It is straightforward to identify a collection of product disks for F: the boundary of a disk D_j will be entirely contained in $\mathbb{b}_j$, $\mathbb{b}_k$ (the next band of the same type as $\mathbb{b}_j$), and $S_i \cup S_{i+1} \cup A$ (where S_i and S_{i+1} are the Seifert disks to which $\mathbb{b}_j$ and $\mathbb{b}_k$ are attached). Decomposing X_F along $c_1 + c_2 - 2$ disks results in a single product sutured ball. Since fiber surfaces are minimal genus Seifert surfaces, we conclude $\chi(F) = 3 - (c_1 + c_2)$ and $2g(K) - 1 = c_1 + c_2 - 3$.

Definition 3.5. *Suppose a product disk has boundary contained in $\mathbb{b}_j$ and $\mathbb{b}_k$, which are bands of the same type with $j < k$. We refer to this disk as D_j. Furthermore, we denote the non-sutured portion of ∂D_j, $\overline{\partial D_j - A}$, by $\alpha_j^+ \cup \alpha_j^-$, where $\alpha_j^\star \subset F^\star$.*

The product disk D_j is completely determined by the arcs α_j^- and $\alpha_j^+ \approx \varphi(\alpha_j^-)$, so we use these arcs to identify product disks – in particular, we will not include the interior of these disks in our figures. As in Figure 9, we draw $\alpha_j^\pm$ on $F \times \left\{\frac{1}{2}\right\}$, not in $(X_F, K \times I)$.

3.2 Foundations and the $P(-2,3,7)$ pretzel knot

This section provides the structure of proof of Theorem 1.15 and a series of important lemmas towards that end. We establish notation for constructing and analyzing branched surfaces in exteriors of positive 3-braid closures. The proof of Theorem 1.15, in Section 3.3, requires analysis of 3 cases; we carry out the example of $P(-2,3,7)$ here alongside our preparatory material as motivation. This example already contains the richness of the several cases required to prove Theorem 1.15.

We outline the construction of taut foliations in $S^3_r(K)$, K realized as the closure of a positive 3-braid, $r \in (-\infty, 2g(K) - 1)$:

Section 3.2.1: Identify $c_1 + c_2 - 2$ disjoint product disks $\{D_j\}$ in X_F

Section 3.2.2: Isotope $\{D_j\}$ into a standardized position in X_K

Section 3.2.3: Build the spine of the branched surface in X_K from a copy of the fiber surface F and these standardized disks

Section 3.2.4: Build the laminar branched surface B:

- *Section 3.2.5:* Assign optimal co-orientations for the standardized $\{D_j\}$
- *Section 3.2.6:* Check B is sink disk free
- *Section 3.2.7:* Prove B is a laminar branched surface

Section 3.2.8: Construct taut foliations in X_K:

- *Section 3.2.9:* Show the boundary train track τ carries all slopes $r \in (-\infty, 2g(K) - 1)$
- *Section 3.2.10:* Extend essential laminations to taut foliations in X_K
- *Section 3.2.11:* Produce taut foliations in $S^3_r(K)$ via Dehn filling

To begin our motivational example, we note that $P(-2,3,7)$ is the closure of a positive 3-braid. In particular, $P(-2,3,7) = \hat{\beta}$, for $\beta = \sigma_1^7\sigma_2^2\sigma_1^2\sigma_2$.

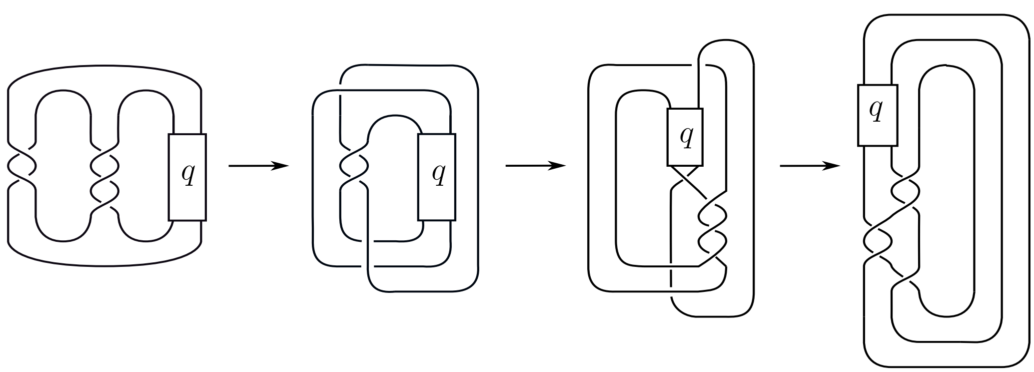

Figure 10: An isotopy of $P(-2,3,q)$, q odd, $q \geq 1$ into the positive closed 3-braid $\hat{\beta}$, for $\beta = \sigma_1^q\sigma_2^2\sigma_1^2\sigma_2$.

3.2.1 Identify disjoint product disks $\{D_j\}$ in X_F.

The setup in Section 3.1 supplies c_1+c_2-2 product disks: take the product disks used to show F is a fiber surface for K.

Figure 11 shows the fiber surface for $P(-2,3,7)$, and 10 product disks $\{D_1,\ldots D_{10}\}$. The disks $\{D_1,D_2,\ldots,D_7,D_{10}\}$ have boundaries contained in $\mathbb{b}_1\cup\ldots\cup\mathbb{b}_7\cup\mathbb{b}_{10}\cup\mathbb{b}_{11}\cup S_1\cup S_2$; the disks $\{D_8,D_9\}$ have boundaries contained in $\mathbb{b}_8\cup\mathbb{b}_9\cup\mathbb{b}_{12}\cup S_2\cup S_3$. The product disks $D_1,\ldots,D_{10}$ are disjoint in X_F, as $\alpha_1^-,\ldots,\alpha_{10}^-$ are pairwise disjoint.

3.2.2 Isotope $\{D_j\}$ into a standardized position in X_K

The c_1+c_2-2 product disks found in Section 3.2.1 are contained in the surface exterior $X_F\approx\overline{X_K-(F\times[\frac{1}{4},\frac{3}{4}])}$. Collapsing $F\times\left[\frac{1}{4},\frac{3}{4}\right]$ to $F\times\left\{\frac{1}{2}\right\}$ produces c_1+c_2-2 disks in X_K, with $\partial D_j\subset(F\times\{1/2\})\cup\partial X_K$.

Consider $(F\times\{\frac{1}{2}\})\cup(D_1\cup\ldots\cup D_{c_1+c_2-2})$ in X_K. This is the spine for a branched surface in X_K. For all $j\neq\ell$ and fixed $\star\in\{+,-\}$, the arcs $\alpha_j^\star$ and $\alpha_\ell^\star$ are disjoint on the fiber surface $F\times\{\frac{1}{2}\}$. However, for $j\neq\ell$, it is possible for α_j^+ and α_ℓ^- to intersect on $F\times\{\frac{1}{2}\}$; after smoothing, there will be many triple points, as in Figure 2.

We want to simplify the forthcoming branched surface. To this end, we isotope the product disks $D_1,\ldots,D_{c_1+c_2-2}$ in X_K such that the arcs $\{\alpha_j^\pm\}$ intersect minimally on $F\times\{\frac{1}{2}\}$.

There are two types of intersection points between α_j^+ and α_ℓ^-, $j\neq\ell$:

Definition 3.6. *A* ***Type 1 intersection point*** *arises from $\alpha_j^+\cap\alpha_{j+1}^-$, where $\mathbb{b}_j$ and $\mathbb{b}_{j+1}$ are bands of the same type. A* ***Type 2 intersection point*** *arises from $\alpha_j^+\cap\alpha_\ell^-$, where $\mathbb{b}_j$ and $\mathbb{b}_\ell$ are bands associated to the last occurrences of σ_1 and σ_2 in the same block $\sigma_1^{a_i}\sigma_2^{b_i}$.*

In Figure 11, we see nine triple points in the spine of $P(-2,3,7)$: there are eight Type 1 intersection points, and a single Type 2 intersection point. Lemma 3.9 will eliminate all Type 1 intersection points.

Definition 3.7. *Let D_j be a product disk in the spine of a branched surface. A **spinal isotopy** $\iota_j : D_j \times [0,1] \to X_K$ is an isotopy of the disk D_j in X_K such that for all $t \in [0,1]$,*

- $\iota_j|_{\alpha_j^- \times \{t\}} = \mathbb{1}$
- $\iota_j(\alpha_j^+ \times \{t\}) \subset (F \times \{\frac{1}{2}\})^+$
- $(\partial D \cap \partial X_K) \subset \partial X_K$
- $\mathring{D} \subset X_K - (F \times \{\frac{1}{2}\})$

and $\iota_j(\alpha_j^+ \times \{1\}) \subset S_i$, where $i = 2, 3$.

Intuitively, allowing α_j^+ to move freely along $F \times \{\frac{1}{2}\}$ guides an isotopy of D_j in X_K.

Definition 3.8. *An arc α_j^+ is in **standard position** if it has been isotoped to lie entirely in a single Seifert disk $S_i, i = 2, 3$. A disk is in **standard position** if both α_j^+ and α_j^- lie entirely in $S_1 \cup S_2 \cup S_3$.*

Lemma 3.9. *There exists a sequence of $c_1 + c_2 - 2$ spinal isotopies of the disks $D_1, \ldots, D_{c_1+c_2-2}$ putting all disks in standard position. Equivalently, there exists a splitting of the spine of the branched surface with no Type 1 intersection points, i.e. with $\alpha_1^+, \ldots, \alpha_{c_1+c_2-2}^+$ in standard position.*

Proof. Scanning the diagram of $F \times \{\frac{1}{2}\}$ from bottom to top, find the first arc α_s^+ encountered. The last letter of β is σ_2, so $\alpha_s^+ \subset \mathbb{b}_s \cup \mathbb{b}_{c_1+c_2} \cup S_2 \cup S_3$, with $s < c_1 + c_2$. If we allow *free* isotopy of arcs in $F \times \frac{1}{2}$ (i.e. an isotopy i_s of α_s^+ where the endpoints of the arc can move along ∂F), α_s^+ can be isotoped to lie entirely in S_3. Let ι_s be the spinal isotopy of D_s in X_K such that for all t, $\iota_s(\alpha_s^+ \times \{t\}) = i_s(\alpha_s^+ \times \{t\})$. Applying ι_s puts D_s in standard position.

Continue scanning the diagram from bottom to top, and find the next arc α_r^+ encountered. Apply the spinal isotopy ι_r of D_r in X_K such that $\iota_r|_{\alpha_r^+\times\{t\}}$ pushes α_r^+ into standard position. After c_1+c_2-2 iterations of this procedure (finding the next arc α_m^+ encountered, and putting the disk D_m in standard position via ι_m), all disks are standardized. A Type 1 intersection between α_t^+ and α_{t+1}^- is eliminated by the isotopy ι_t standardizing D_t. $\square$

Remark 3.10. *The pre- and post- split spine have isotopic exteriors.*

For $P(-2,3,7)$, the arcs get isotoped in the following order:

$$\alpha_9^+, \alpha_{10}^+, \alpha_7^+, \alpha_8^+, \alpha_6^+, \alpha_5^+, \alpha_4^+, \alpha_3^+, \alpha_2^+, \alpha_1^+$$

The result of applying Lemma 3.9 is seen in the right diagram in Figure 11. There is a single Type 2 intersection point between α_7^+ and α_9^-.

Going forward, all disks D_j are in standard position, unless stated otherwise. We will **not** change our notation to indicate the disks are standardized.

3.2.3 Build the spine of the branched surface

The spine for the branched surface is built from

$$(F\times\{1/2\})\cup\left(\bigcup_{i=1}^{c_1+c_2-2} D_i\right)$$

For $P(-2,3,7)$, the spine for the branched surface is in Figure 11.

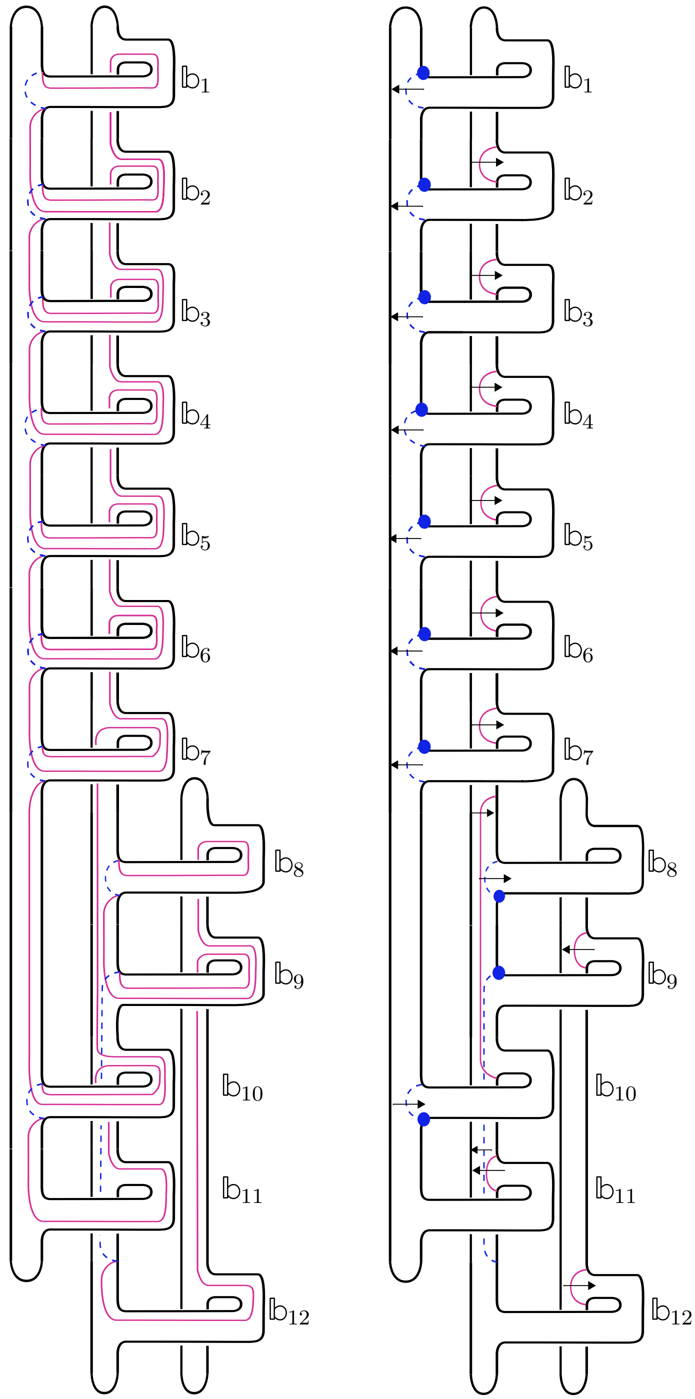

Figure 11: On the left: the fiber surface and 10 product disks for $P(-2,3,7)$. On the right: the laminar branched surface for $P(-2,3,7)$ with cusping directions $(\leftarrow)^7(\rightarrow)(\leftarrow)(\rightarrow)(\ \ )(\ \ )$.

3.2.4 Build the branched surface B

To build the laminar branched surface, we need to assign co-orientations for the disks D_j, $1 \leq j \leq c_1 + c_2 - 2$, and verify these choices do not create sink disks. To achieve these goals, we study the branch locus and branch sectors.

Lemma 3.9 simplified the branch locus: all arcs $\alpha_j^{\pm}$, $1 \leq j \leq c_1 + c_2 - 2$ are now contained in $S_1 \cup S_2 \cup S_3$. Moreover, arcs α_j^- are isotopic to the co-cores of bands $\mathbb{b}_j$, or would be if other bands were not obstructing the path of the lower endpoint.

For $P(-2,3,7)$,

- the arcs $\alpha_1^-, \ldots, \alpha_7^-, \alpha_{10}^-$, contained in S_1, are isotopic to the co-cores of the 1-handles $\mathbb{b}_1, \ldots, \mathbb{b}_7, \mathbb{b}_{10}$ respectively.
- the arc α_8^- is isotopic to the co-core of $\mathbb{b}_8$.
- the arcs $\alpha_1^+, \ldots, \alpha_6^+, \alpha_{10}^+$ are isotopic to the co-cores of the 1-handles $\mathbb{b}_2, \ldots \mathbb{b}_7, \mathbb{b}_{11}$, respectively, and are contained in S_2.
- the α_8^+ is isotopic to the co-core of $\mathbb{b}_9$, and is contained in S_3.
- the two arcs α_9^- and α_7^+ are not isotopic to the co-cores of any bands.

Cusp directions for the disks have yet to be assigned. Nevertheless, we know the branch sectors for B will fall into two categories: the sectors that lie in $F \times \{\frac{1}{2}\}$, and sectors arising from isotoped product disks. The former can be further refined into 3 categories:

Definition 3.11. *The S_i **disk sector** is the connected component of a branch sector containing the Seifert disk S_i. A **band sector** is the connected component of a branch sector associated to a positively twisted band. The remaining branch sectors are **polygon sectors**; each lies in a single Seifert disk.*

In particular, all polygon sectors lie in S_2. For $P(-2,3,7)$, there are 7 band sectors (the branch sectors containing $\mathbb{b}_2, \ldots, \mathbb{b}_7 \cup \mathbb{b}_9 \cup \mathbb{b}_{10}$), and a pair of polygon sectors.

3.2.5 Assign optimal co-orientations to $\{D_j\}$

Definition 3.12. *Let $\widehat{\alpha}_j^\star$ denote the cusp direction of $\alpha_j^\star$, for $\star \in \{+,-\}$.*

Lemma 3.13. *Assigning a co-orientation to D_j determines the cusp orientation to both α_j^+ and α_j^-. Moreover, if we orient the arcs $\alpha_j^\pm$ from the lower endpoint to the upper endpoint, the pairings $\langle \alpha_j^+, \widehat{\alpha}_j^+ \rangle$ and $\langle \alpha_j^-, \widehat{\alpha}_j^- \rangle$ have opposite signs.*

Heuristically: the induced cusp orientations of α_j^+ and α_j^- "point in opposite directions" when looking at $(F \times \{\frac{1}{2}\})^+$.

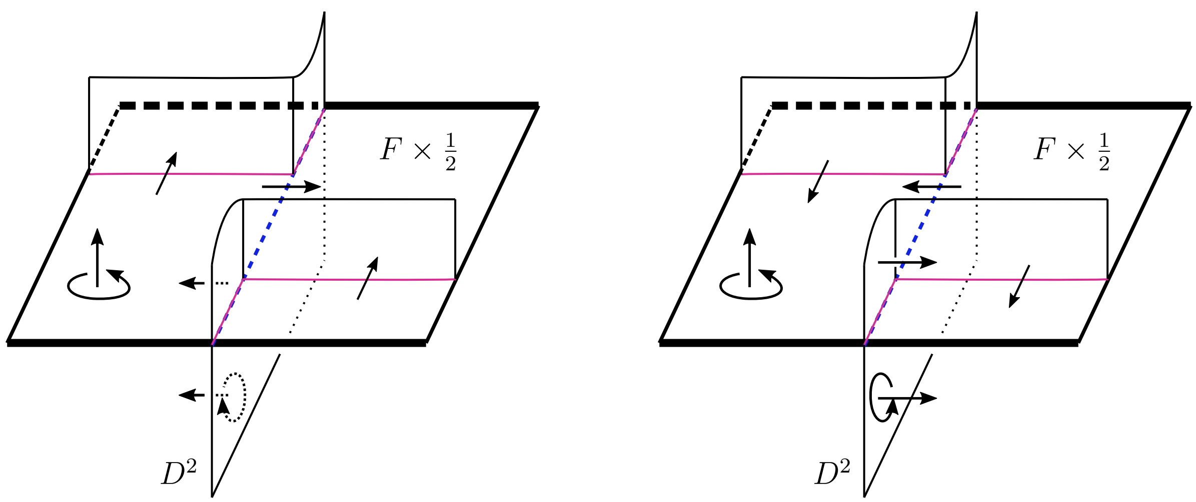

Figure 12: In this local model, we have fixed a co-orientation on $F \times \{\frac{1}{2}\}$, and chosen different co-orientations on D_j in the left and right figures. The correct cusping choices for $\alpha_j^\pm$ are provided. The **bolded** horizontal lines lie on ∂X_K.

Proof. For simplicity, assume the disk has yet to be standardized. Choose a co-orientation on D_j. Since F is co-oriented, the correct smoothing choices for α_j^+ and α_j^- ensure the co-orientations of F and D_j agree near the branch locus. The corresponding cusp directions for $\alpha_j^{\pm}$ can be determined immediately, as in the local model in Figure 12: if the cusp direction on α_j^- points to the right (resp. left) near ∂X_K, then the cusp direction on α_j^+ points to the left (resp. right) near ∂X_K. Taking a global viewpoint as in Figure 13, orient the arcs $\alpha_j^{\pm}$ from the lower endpoint to the upper endpoint: the pairings $\langle \alpha_j^{\pm}, \widehat{\alpha}_j^{\pm} \rangle$ have opposite signs, and the cusp directions point in opposite directions when looking at $(F \times \{\frac{1}{2}\})^+$. Our isotopy ι_t of D_t preserves the relative positions of the upper and lower endpoints of α_t^+, so the lemma holds for standardized disks. $\square$

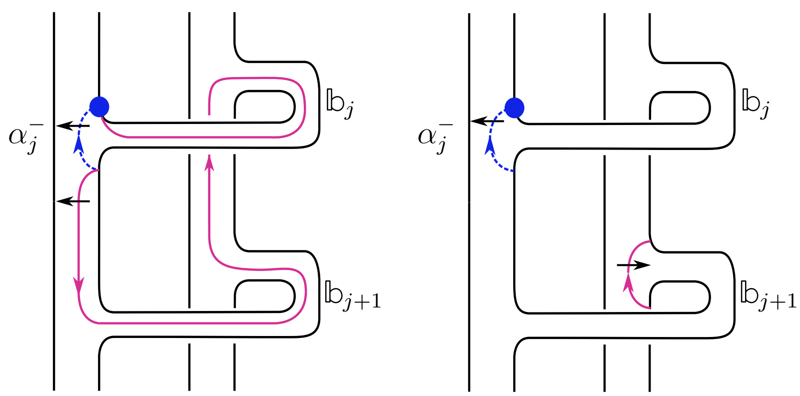

Figure 13: After standardizing, $\widehat{\alpha}_j^-$ and $\widehat{\alpha}_j^+$ “point in opposite directions".

Remark 3.14. *In addition to establishing conventions about cusp directions, Figure 13 indicates special (i.e. bolded) endpoints. The meaning of the bolding is postponed until Definition 3.19 (it will become relevant when computing the slopes carried by the branched surface).*

The cusp direction of α_j^- determines the co-orientation of D_j. Moreover, the upper endpoint of α_j^- is planted above the attachment site of the 1-handle $\mathbb{b}_j$, which in turn is associated to the j^{th} letter σ_i of β. Therefore, we can encode the co-orientation of D_j directly to $\mathbb{b}_j$, via the induced cusp orientation on α_j^-.

Definition 3.15. *We encode the co-orientation of D_j by recording the cusp direction of α_i^- in tandem with β. For σ the j^{th} letter of β:*

- *Writing $\leftarrow$ below σ indicates $\langle \widehat{\alpha}_j^-, \alpha_j^- \rangle = 1$ and $\langle \widehat{\alpha}_j^+, \alpha_j^+ \rangle = -1$. That is, α_j^- is cusped "to the left", and α_j^+ is cusped "to the right" when looking at $(F \times \{\frac{1}{2}\})^+$.*

- *Writing $\rightarrow$ below σ indicates $\langle \widehat{\alpha}_j^-, \alpha_j^- \rangle = -1$ and $\langle \widehat{\alpha}_j^+, \alpha_j^+ \rangle = 1$. That is, α_j^- is cusped "to the right", and α_j^+ is cusped "to the left" when looking at $(F \times \{\frac{1}{2}\})^+$*

- *Writing ( ) below σ indicates **not** choosing the product disk D_j with pre-standardized arc α_j^+ passing through this 1-handle. We say σ is **uncusped**.*

$P(-2,3,7)$ is realized as the closure of $\beta = \sigma_1^7\sigma_2^2\sigma_1^2\sigma_2 = \sigma_1^7\sigma_2\sigma_2\sigma_1\sigma_1\sigma_2$. The cusping directions in (3.2) below determine a branched surface – it specifies which product disks to choose when building the spine, and how to co-orient them, as in Figure 11.

$$\begin{array}{cccccc} \sigma_1^7 & \sigma_2 & \sigma_2 & \sigma_1 & \sigma_1 & \sigma_2 \\ (\leftarrow)^7 & (\rightarrow) & (\leftarrow) & (\rightarrow) & (\quad) & (\quad) \end{array} \tag{3.2}$$

We emphasize: directions, as in (3.2), completely determine a branched surface. In Section 3.3.2, we assign cusp directions for an arbitrary positive 3-braid closure.

3.2.6 Check B is sink disk free

Lemma 3.16. *A branch sector arising from an isotoped product disk is never a sink disk.*

Proof. Let D_j be any product disk sector. By Lemma 3.13, the pairings $\langle \alpha_j^+, \widehat{\alpha}_j^+ \rangle$ and $\langle \alpha_j^-, \widehat{\alpha}_j^- \rangle$ have opposite signs. Therefore, one of $\widehat{\alpha}_j^+$ and $\widehat{\alpha}_j^-$ points out of $(F \times \{\frac{1}{2}\})^+$ and into D_j (and vice-versa for the other). It is impossible for both cusp directions to point into D_j. $\square$

In Section 3.3, we develop techniques for determining which cusping directions (as in (3.2)) create sink disks. For the branched surface B for $P(-2,3,7)$, we already identified the branch sectors on $F \times \{\frac{1}{2}\}$, so verifying B is sink disk free is straightforward. To show a branch sector is not a half sink disk, we need only check some cusped arc $\widehat{\alpha}_j^\star$ points out of it.

- The Disk Sectors
  - S_1 is not a sink disk, because $\widehat{\alpha}_{10}^-$ points out of it.
  - S_2 is not a sink disk, because $\widehat{\alpha}_1^+$ points out of it.
  - S_3 is not a sink disk, because $\widehat{\alpha}_9^+$ points out of it.
- The Band Sectors
  - The sectors $\mathbb{b}_2, \ldots, \mathbb{b}_7$ have $\widehat{\alpha}_2^-, \ldots, \widehat{\alpha}_7^-$ pointing out of the respective regions.
  - The band sector containing $\mathbb{b}_9 \cup \mathbb{b}_{10}$ in the boundary has $\widehat{\alpha}_9^-$ pointing out of it.
- The Polygon Sectors
  - The boundary of the **upper polygon sector** P_u is contained in $\alpha_7^+ \cup \alpha_8^- \cup \alpha_9^- \cup \partial F$; $\widehat{\alpha}_8^-$ points out of the sector.
  - The boundary of the **lower polygon sector** P_ℓ is contained in $\alpha_7^+ \cup \alpha_9^- \cup \alpha_{10}^+ \cup \partial F$; $\widehat{\alpha}_9^-$ points out of the sector.

3.2.7 B is a laminar branched surface

Proposition 3.17. *A sink disk free branched surface B, constructed from a copy of the fiber surface and a collection of product disks, is a laminar branched surface.*

Proof. We verify B is laminar by verifying conditions (1) – (4) of Theorem 2.4 hold. Note that the M of Theorem 2.4 is X_K.

(1a) $\partial_h(N(B))$ **is incompressible and** ∂**-incompressible in** $M - \textbf{int}(N(B))$**.**

A sutured manifold (M, γ) is **taut** if M is irreducible and $R(\gamma)$ is norm minimizing in $H_2(M, \gamma)$ [Gab83]. Each of our product disks appears in a sutured manifold decomposition of $(X_F, K \times I)$ which terminates in $(D^2, S^1 \times I)$. Thus, any sutured manifold appearing in the sequence of product disk decompositions of $(X_F, K \times I)$ is a taut sutured manifold [Gab83]. In particular, the exterior of the pre-split spine (built from $c_1 + c_2 - 2$ co-oriented product disks), (M', γ'_M), is a taut product sutured manifold, and $R(\gamma'_M)$ is norm minimizing.

The exterior of the post-split spine also has a product sutured manifold structure; denote this manifold (N', γ'_N). For B the branched surface whose spine has standardized disks, we have $\gamma'_N \approx \partial_v(N(B)) \cup (\partial X_K - int(N(B))|_{\partial X_K})$ and $R(\gamma'_N)$ is isotopic to $R(\gamma'_M) \approx \partial_h(N(B))$. Thus $\partial_h N(B)$ is norm minimizing in $H_2(N', \gamma'_N)$, and $\partial_h(N(B))$ is incompressible and ∂-incompressible in $M - int(N(B))$.

(1b) **There is no monogon in** $M - \textbf{int}(N(B))$**.**

This follows from our construction; the branched surface has a transverse orientation.

(1c) **No component of** $\partial_h N(B)$ **is a sphere or a disk properly embedded in** M**.**

Every component of $\partial_h N(B)$ meets ∂X_K, so no component of $\partial_h(N(B))$ can be a sphere. The horizontal boundary $\partial_h N(B)$ is properly embedded in X_B, not X_K.

(2) $M - \textbf{int}(N(B))$ **is irreducible and** $\partial M - \textbf{int}(N(B))$ **is incompressible in** $M - \textbf{int}(N(B))$**.**

$M - int(N(B))$ is a submanifold of S^3 with connected boundary, thus is irreducible. $\partial X_K - int(N(B))$ is a torus with a neighborhood of a train track removed: it is a collection of bigons. In particular, any simple closed curve in $\partial X_K - int(N(B))$ bounds a disk in $\partial X_K - int(N(B))$, and is incompressible in $M - int(N(B))$.

(3) B **contains no Reeb branched surface (see [GO89] for more details).** To prove B does not contain a Reeb branched surface, it suffices to show that B cannot carry a torus or fully carry an annulus.

By construction, every sector of B meets ∂X_K. Thus, any compact surface carried by B must also meet ∂X_K. Thus, B cannot carry a torus.

We now prove B cannot fully carry an annulus. Suppose, by way of contradiction, that B fully carries a compact surface S. Any such S is built as a union of branch sectors, where each branch sector has a positive weight. Since β is in the form specified by Section 3.1, we can restrict our attention to the first two letters of the braid word, namely $\sigma_1\sigma_1$; see Figure 14. We assign weights to the relevant branch sectors:

- the disk sectors D_1 and D_2 have weights w_1 and w_2, respectively
- the band sector $\mathbb{b}_2$ has weight w_3,
- the two (isotoped) product disks associated to σ_1^2 have weights w_4 and w_5.

See Figure 14. If B carries a compact surface, the switch relations induced by the branch loci induce the following: $w_1 = w_2 + w_4$, $w_3 = w_2 + w_4$, and $w_1 = w_5 + w_3$.

This implies that $w_1 = w_3 = w_3 + w_5$, thus $w_5 = 0$. This contradicts that S is fully carried by B. We conclude that B cannot carry any compact surface, and therefore does not carry an annulus.

(4) B **is sink disk free.**

This holds by assumption. □

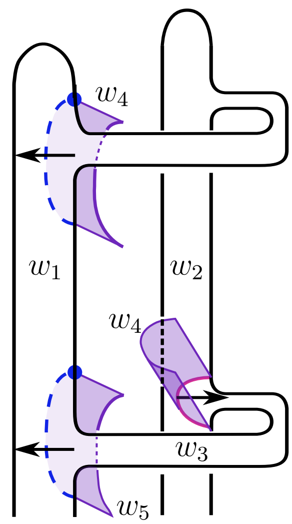

Figure 14: A local picture of the branched surface near the bands $\mathbb{b}_1$ and $\mathbb{b}_2$. For simplicity, the product disk associated to α_1 appears broken in our figure; it has weight w_4. The standard relations near the branch locus indicate that $w_5 = 0$, thus B cannot fully carry an annulus.

3.2.8 Construct taut foliations in X_K

B is a laminar branched surface. Theorem 2.4 guarantees that for every rational slope r carried by the boundary train track τ, there exists an essential lamination $\mathcal{L}_r$ meeting ∂X_K in simple closed curves of slope r. To construct taut foliations in X_K, we first understand which slopes are carried by τ, apply Theorem 2.4 to get a family of essential laminations, and then extend each lamination to a taut foliation in X_K.

3.2.9 Show the train track τ carries all rational slopes $r < 2g(K) - 1$

Since B is formed by $(F \times \{\frac{1}{2}\}) \cup D_1 \cup \ldots \cup D_{c_1+c_2-2}$, the boundary train track τ carries slope 0.

Definition 3.18. *Each D_j meets ∂X_K in two arcs, each tracing out the path of an endpoint of α_j^- under φ. These arcs are* ***sectors of the train track*** *τ; $\overline{\tau - \lambda}$ is a collection of sectors.*

We have $c_1 + c_2 - 2$ disks, and therefore $2 \cdot (c_1 + c_2 - 2)$ sectors in the associated train track τ. Consider α_j^- with cusping $\widehat{\alpha}_j^-$. The cusping $\widehat{\alpha}_j^-$ will agree with the orientation of λ at one endpoint of α_j^-, and disagree at the other endpoint. Thus, for s_j and s_j' the pair of sectors induced by α_j^-, the train tracks $\lambda \cup s_j$ and $\lambda \cup s_j'$ carry different slopes, as in Figure 15: $\lambda \cup$ (the leftmost sector) carries $[0, 1)$, while $\lambda \cup$ (the middle sector) carries $(-\infty, 0]$.

Definition 3.19. *If the direction of $\widehat{\alpha}_j^-$ disagrees with the orientation of λ at a given endpoint of α_j^-, we say this endpoint* ***contributes maximally to*** *τ.*

In our figures, the endpoint of α_j^- contributing maximally is **bolded**.

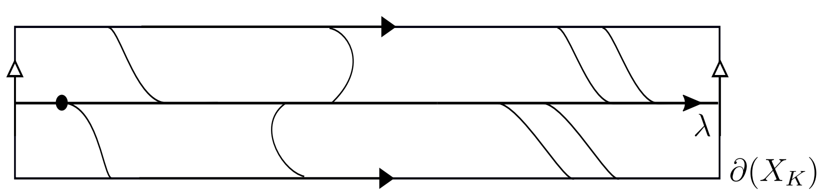

Figure 15: A train track $\tau \subset \partial(X_K)$. $\lambda \cup$ (the leftmost sector) carries $[0, 1)$, while $\lambda\cup$ (the middle sector) carries $(-\infty, 0]$. The rightmost sectors are linked.

Our goal is to maximize the interval of slopes carried by τ. There are $c_1 + c_2 - 2$ endpoints contributing maximally to τ – one for each product disk. It is tempting to claim τ carries all slopes $[0, c_1 + c_2 - 2)$. However, this is naïve: the endpoints of the arcs α, α' could be linked on along ∂F, as in the rightmost picture in Figure 15.

Definition 3.20. *Let α_j^- and α_ℓ^- be distinct properly embedded arcs on F such that (1) the first endpoint of each arc contributes maximally to τ and (2) their endpoints are linked in λ. Then α_j^- and α_ℓ^- are called* ***linked arcs****. See Figure 15. If α_j^- and α_ℓ^- are not linked, they are* ***unlinked*** *or* ***not linked****.*

The train track τ induced by B will carry all slopes in $(-\infty, k)$, where k is the maximum number of pairwise unlinked arcs contributing maximally to τ. Proving Theorem 1.15 requires sorting positive 3-braids into three types. For each type, we construct a laminar branched surface B using $c_1 + c_2 - 2$ product disks and a unique pair of linked arcs. Thus, τ carries all slopes in $[0, (c_1 + c_2 - 2) - 1) = [0, 2g(K) - 1)$.

Definition 3.21. *A* ***sub-train-track*** *τ' of τ is a train track carrying slope 0, such that $\{$sectors of $\tau'\} \subseteq \{$sectors of $\tau\}$.*

Remark 3.22. *For our purposes, τ' will include all sectors contributing maximally to τ, and a single sector s with $\lambda \cup s$ carrying $(-\infty, 0]$.*

Lemma 3.23. *Any slope carried by τ', a sub-train-track of τ, is also carried by τ.* $\square$

For $P(-2,3,7)$, we have $c_1 + c_2 - 2 = 10$ sectors contributing maximally to τ, and exactly one pair of linked arcs coming from α_8^- and α_9^-. Let τ' be the sub-train-track built from the endpoints of $\alpha_1^-, \ldots, \alpha_{10}^-$ that contribute maximally to τ. Thus τ' carries all rational slopes in $[0, 9)$. Appending the upper endpoint of α_8^- to τ' ensures τ' carries all slopes in $(-\infty, 9)$. Applying Lemma 3.23, we conclude τ, the train track induced by B, carries slopes in $(-\infty, 9)$.

3.2.10 Extend essential laminations to taut foliations

We now have a laminar branched surface B carrying all rational slopes in $(-\infty, 2g(K)-1)$. By Theorem 2.4, B carries an essential lamination $\mathcal{L}_r$ for every rational $r \in (-\infty, 2g(K)-1)$. We use these laminations to construct taut foliations in X_K.

Proposition 3.24. *Let $\mathcal{L}_r$ be an essential lamination carried by our laminar branched surface B, such that $\mathcal{L}_r$ meets ∂X_K in simple closed curves of slope r. Then $\mathcal{L}_r$ can be extended to a taut foliation in X_K, which foliates ∂X_K in parallel simple closed curves of slope r.*

Proof. In Proposition 3.17, we proved the branched surface exterior $X_B \approx \overline{X_K - int(N(B))}$ is isotopic to a product sutured manifold. In particular, X_B has an I-bundle structure. $N(B)$ is an I-bundle over B, thus $\overline{N(B) - \mathcal{L}_r}$ has an I-bundle structure. Endowing the lamination exterior $X_{\mathcal{L}_r} \approx \overline{X_K - \mathcal{L}_r}$ with an I-bundle structure yields a foliation $\mathcal{F}_r$ for X_K which is induced by $\mathcal{L}_r$.

$\mathcal{L}_r$ meets ∂X_K in simple closed curves of slope r, so $\overline{X_{\mathcal{L}_r}}|_{\partial X_K}$ is an r-sloped annulus A_r. A_r is formed from $X_B|_{\partial X_K}$ and $\overline{N(B) - L_r}|_{\partial X_K}$, which both have I-bundle structures. Simultaneously endowing X_B and $\overline{N(B) - L_r}$ with an I-bundle structure (as above) foliates A_r by circles of slope r; thus ∂X_K is foliated by simple closed curves of slope r. □

3.2.11 Produce taut foliations in $S^3_r(K)$ via Dehn filling

For all rational $r < 2g(K)-1$, X_K admits a taut foliation $\mathcal{F}_r$ foliating ∂X_K in simple closed curves of slope r. Performing r-framed Dehn filling endows $S^3_r(K)$ with a taut foliation.

To summarize for $P(-2,3,7)$: we constructed a laminar branched surface $B \subset X_K$. The induced train track τ carries all rational slopes in $(-\infty, 2g(K)-1) = (-\infty, 9)$. Applying Proposition 3.17, Theorem 2.4 and Proposition 3.24, we deduce

X_K admits taut foliations meeting the boundary torus T in simple closed curves of slope $r \in (-\infty, 2g(K)-1)$. Performing r-framed Dehn filling yields $S^3_r(K)$ endowed with a taut foliation. These manifolds are non-L-spaces; we have produced the taut foliations predicted by Conjecture 1.14.

3.3 Proving the positive 3–braids theorem

In this section, we prove:

Theorem 1.15. *Let K be a knot in S^3, realized as the closure of a positive 3-braid. Then for every rational $r < 2g(K)-1$, the knot exterior $X_K := S^3 - \mathring{\nu}(K)$ admits taut foliations meeting the boundary torus T in parallel simple closed curves of slope r. Hence the manifold obtained by r-framed Dehn filling, $S^3_r(K)$, admits a taut foliation.*

The proof requires generalizing the $P(-2,3,7)$ example of Section 3.2. In Section 3.3.1, we prove a few lemmas. Three families of branched surfaces are constructed in Section 3.3.2.

3.3.1 Co-orienting Arcs

Given an arbitrary positive 3-braid word β, we choose $c_1 + c_2 - 2$ product disks, as in Section 3.2.1. We need a strategy for assigning co-orientations. As in Section 3.2.5, we will provide cusp directions in tandem with β, and analyze which cusping directions produce sink disks and linked arc pairs. We aim to maximize the slopes carried by τ while ensuring B is sink disk free.

Lemma 3.25. *Suppose the subword $\sigma_i\sigma_i$ arises as the j^{th} and $j+1^{st}$ letters in β. The cusping directions $(\leftarrow)^2, (\rightarrow)^2$, and $(\rightarrow\leftarrow)$ prevent the band sector $\mathbb{b}_{j+1}$ from being a half sink disk.*

Proof. As in Figures 16 and 18, α_j^+ is isotopic to the co-core of $\mathbb{b}_{j+1}$. If $\widehat{\alpha}_j^- = (\rightarrow)$, then by Lemma 3.13, $\widehat{\alpha}_j^+ = (\leftarrow)$, hence the directions $(\rightarrow)^2$ and $(\rightarrow\leftarrow)$ do not make $\mathbb{b}_{j+1}$ a half sink disk. The cusping directions $(\leftarrow)^2$ have $\widehat{\alpha}_{j+1}^-$ pointing out of $\mathbb{b}_{j+1}$. $\square$

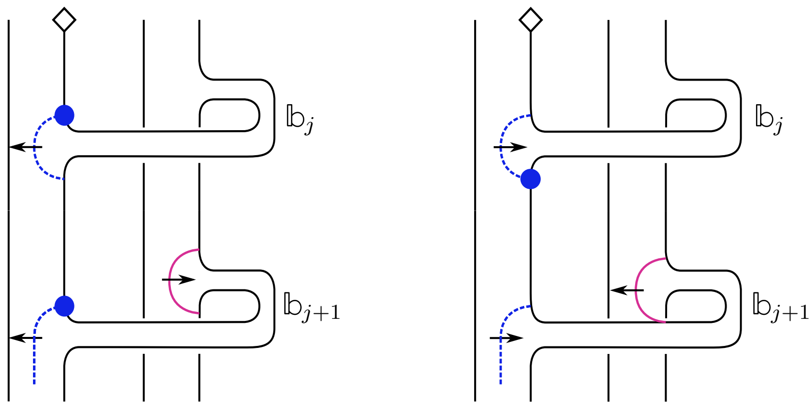

Figure 16: The directions $(\rightarrow)^2$ and $(\leftarrow)^2$ do not make $\mathbb{b}_{j+1}$ a half sink disk.

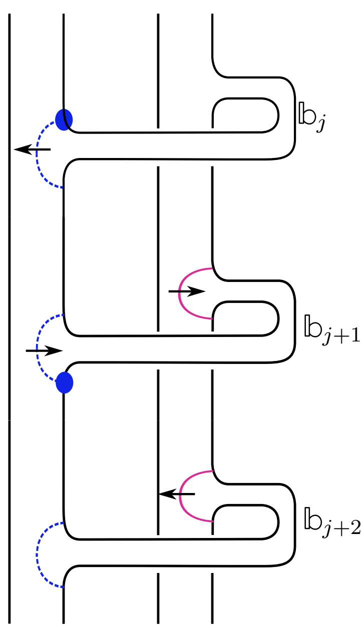

Figure 17: The band $\mathbb{b}_{j+1}$ is a half sink disk.

Lemma 3.26. *Suppose β contains the subword $\sigma_i\sigma_i\sigma_i$, arising as the $j, j+1, j+2$ letters of β. The cusping directions* $(\leftarrow \quad \rightarrow \quad \star\ )$, $\star \in \{\rightarrow, \quad \leftarrow, \quad \}$ *force* $\mathbb{b}_{j+1}$ *to be a half sink disk.*

Proof. As in Figure 17, both α^-_{j+1} and α^+_j are isotopic to the co-core of $\mathbb{b}_{j+1}$. Not only does $\widehat{\alpha}^-_{j+1}$ point into $\mathbb{b}_{j+1}$, but by Lemma 3.13, so does $\widehat{\alpha}^-_{j+1}$. $\square$

To produce a sink disk free branched surface, we should avoid the cusp directions $(\leftarrow \quad \rightarrow)$.

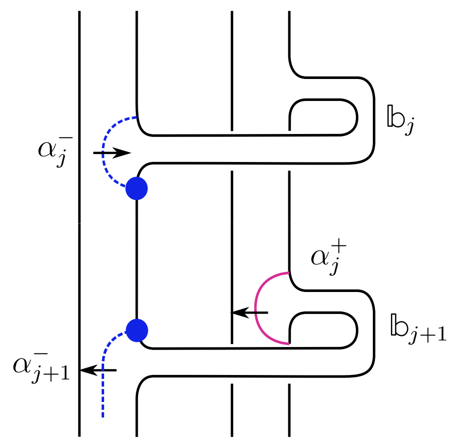

Figure 18: The arcs α^-_j and α^-_{j+1} are linked.

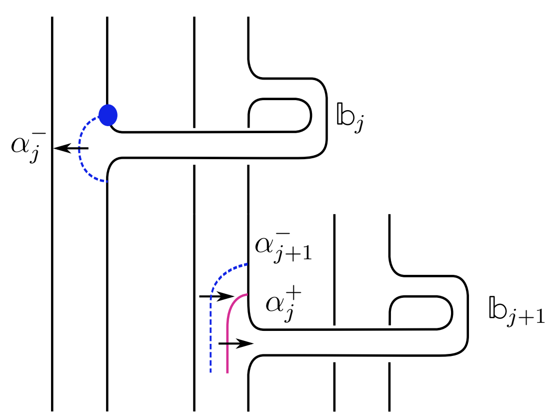

Figure 19: The arcs α^-_j and α^-_{j+1} are not linked.

Lemma 3.27. *Suppose β contains the subword $\sigma_i\sigma_i$ arising as the j^{th} and $j+1^{st}$ letters in the braid word β. The associated cusping directions $(\leftarrow\ \leftarrow)$ and $(\rightarrow\ \rightarrow)$ create an arc, unlinked from all other arcs, that contributes maximally to τ. The cusping directions $(\rightarrow\ \leftarrow)$ create a pair of linked arcs.*

Proof. First, suppose $(\sigma_i)^2$ is cusped via $(\leftarrow)^2$, as in the left picture in Figure 16. The bolded endpoints of α_j^- and α_{j+1}^- contribute maximally to τ. Traversing K from $\Diamond$, we first encounter the upper endpoint of α_j^-, and then its image: no point that contributes maximally to τ occurs between them. Thus α_j^- is unlinked from all other arcs. Analogously, if $(\sigma_i)^2$ is cusped via $(\rightarrow)^2$, α_j^- is unlinked from all other arcs, as in the right picture of Figure 16. If $(\sigma_i)^2$ is cusped via $(\rightarrow\ \leftarrow)$, α_j^- and α_{j+1}^- are linked, as in Figure 18. $\square$

Lemma 3.28. *Suppose the subword $\sigma_1\sigma_2$ occurs as the j and $j+1$ letters of β. The arcs α_j and α_{j+1}, cusped as $(\leftarrow\ \rightarrow)$, are unlinked.*

Proof. As in Figure 19, α_j^- is unlinked from α_{j+1}. $\square$

3.3.2 Building Branched Surfaces

Definition 3.29. *β has the form described in Equation 3.1. Then β is one of Types A, B, or C described below:*

***Type A**: $k=1$, and $\beta=\sigma_1^{a_1}\sigma_2^{b_1}$. For $\hat{\beta}$ to be a knot, a_1 and b_1 are both odd.*

Note: $\hat{\beta}=T(2,a_1)\#T(2,b_1)$.

***Type B**: $k=2$, and $b_1=b_2=1$. So, $\beta=\sigma_1^{a_1}\sigma_2\sigma_1^{a_2}\sigma_2$*

***Type C**: all other positive 3-braid closures; namely:*

- *$k=2$ and (up to cyclic rotation) $a_1,a_2,b_1\geq 2, b_2\geq 1$*
- *$k\geq 3, a_i\geq 2, b_i\geq 1$ for all i.*

Given a positive 3-braid knot, we construct a branched surface by fusing c_1+c_2-2 product disks to $F\times\{\frac{1}{2}\}$, such that we have exactly one linked pair of arcs.

Propositions 3.30, 3.32, 3.33 construct the branched surfaces for **Types A, B, and C** respectively.

Proposition 3.30. *(Building the branched surface for **Type A**)*
Suppose $\beta = \sigma_1^{a_1}\sigma_2^{b_1}$ for a_1, b_1 odd, and $K = \hat{\beta}$. There exists a sink-disk free branched surface $B \subset X_K$, for $K = T(2, a_1)\#T(2, b_1)$, with exactly one pair of linked arcs. Moreover, there exists a sub-train-track τ' of τ carrying all rational slopes $r < 2g(K)-1$.

Proof. First suppose $a_1, b_1 \geq 3$. We identify $c_1 + c_2 - 2 = a_1 + b_1 - 2$ product disks:

$$\begin{array}{rccccc} \beta = \sigma_1^{a_1}\sigma_2^{b_1} = & \sigma_1^{a_1-1} & \sigma_1 & \sigma_2^{b_1-2} & \sigma_2 & \sigma_2 \\ & (\rightarrow)^{a_1-1} & (\ ) & (\rightarrow)^{b_1-2} & (\leftarrow) & (\ ) \end{array} \tag{3.3}$$

The spine of the branched surface is built from $F \times \{\frac{1}{2}\}$, fused with the product disks specified. Applying Lemma 3.9 puts the product disks into standardized position; cusping as== instructed in (3.3) yields a branched surface B. In this case, all arcs on $F \times \frac{1}{2}$ are pairwise unlinked (see Figure 20 for an example). Lemma 3.16 guarantees no product disk sector is a half sink disk, while Lemmas 3.25 and 3.26 guarantee no band sectors are half sink disks. There are no polygon sectors. We check the disk sectors S_1, S_2, and S_3 are not half sink disks.

- $\widehat{\alpha}_1^-$ points out of S_1.
- $\widehat{\alpha}_{a_1+1}^-$ points out of the S_2 disk sector.
- $\widehat{\alpha}_{a_1+b_1-1}^-$ points into the S_2 disk sector, so $\widehat{\alpha}_{a_1+b_1-1}^+$ points out of the S_3 disk sector.

B is sink disk free. By Lemma 3.27, $\alpha_{a_1+b_1-2}^-$ and $\alpha_{a_1+b_1-1}^-$ are the unique pair of linked arcs.

Now suppose $a_1 \geq 3$ and $b_1 = 1$, $a_1 = 1$ and $b_3 \geq 1$, or $a_1 = b_1 = 1$. Then $\hat{\beta}$ is isotopic to $T(2, a_1)$, $T(2, b_1)$, or the unknot respectively. The canonical fiber surface for K is produced after destabilization. The following instructions specify a construction of a branched surface for $T(2, n), n \geq 3$:

$$\begin{array}{rlll} \beta = & \sigma_1^n = \sigma_1^{n-2} & \sigma_1 & \sigma_1 \\ & (\rightarrow)^{n-2} & (\leftarrow) & (\ \ ) \end{array}$$

Standardize the disks as in Lemma 3.9. Lemmas 3.16 and 3.26, and 3.25 guarantee no product disks or band sectors are half sink disks. There are no polygon sectors. $\widehat{\alpha}_1^-$ and $\widehat{\alpha}_{n-1}^+$ point out of S_1 and S_2 respectively, ensuring no disk sectors. Finally, Lemma 3.27 guarantees only α_{n-2}^- and α_{n-1}^- are linked.

Thus for any $\beta = \sigma_1^{a_1}\sigma_2^{b_1}$, $a_1, b_1 \geq 1$ and odd, there exists a sink disk free branched surface B with a unique pair of linked arcs. Including both sectors induced by α_1 to τ' ensures that τ' carries all rational $r < 2g(K) - 1$. $\square$

Remark 3.31. Eventually, we aim to conclude that B is not just sink-disk-free, but that it is laminar. To do so, we need to modify the proof that B does not fully carry an annulus (our proof of this in Proposition 3.17 relied on a local model that does not apply for braids of Type A). However, this is straightforward: consider Figure 14, and reverse the orientations on each of the cusp directions shown (i.e. $\widehat{\alpha}_1^-$ and $\widehat{\alpha}_2^-$ point out of S_1, and $\widehat{\alpha}_1^+$ points into S_2). The resulting local model for a branched surface now matches Type A branched surfaces. We preserve the labelling of the weights of each sector. The new cusp directions, combined with the switch relations at branch sectors, induce the following:

$$w_1 + w_4 = w_2 \qquad w_3 + w_4 = w_2 \qquad w_1 + w_5 = w_3$$

Therefore, $w_1 + w_4 = w_3 + w_4$, which implies $w_1 = w_3$. Again, we conclude that $w_5 = 0$. We conclude that B does not carry any compact surface, and therefore does not carry an annulus.

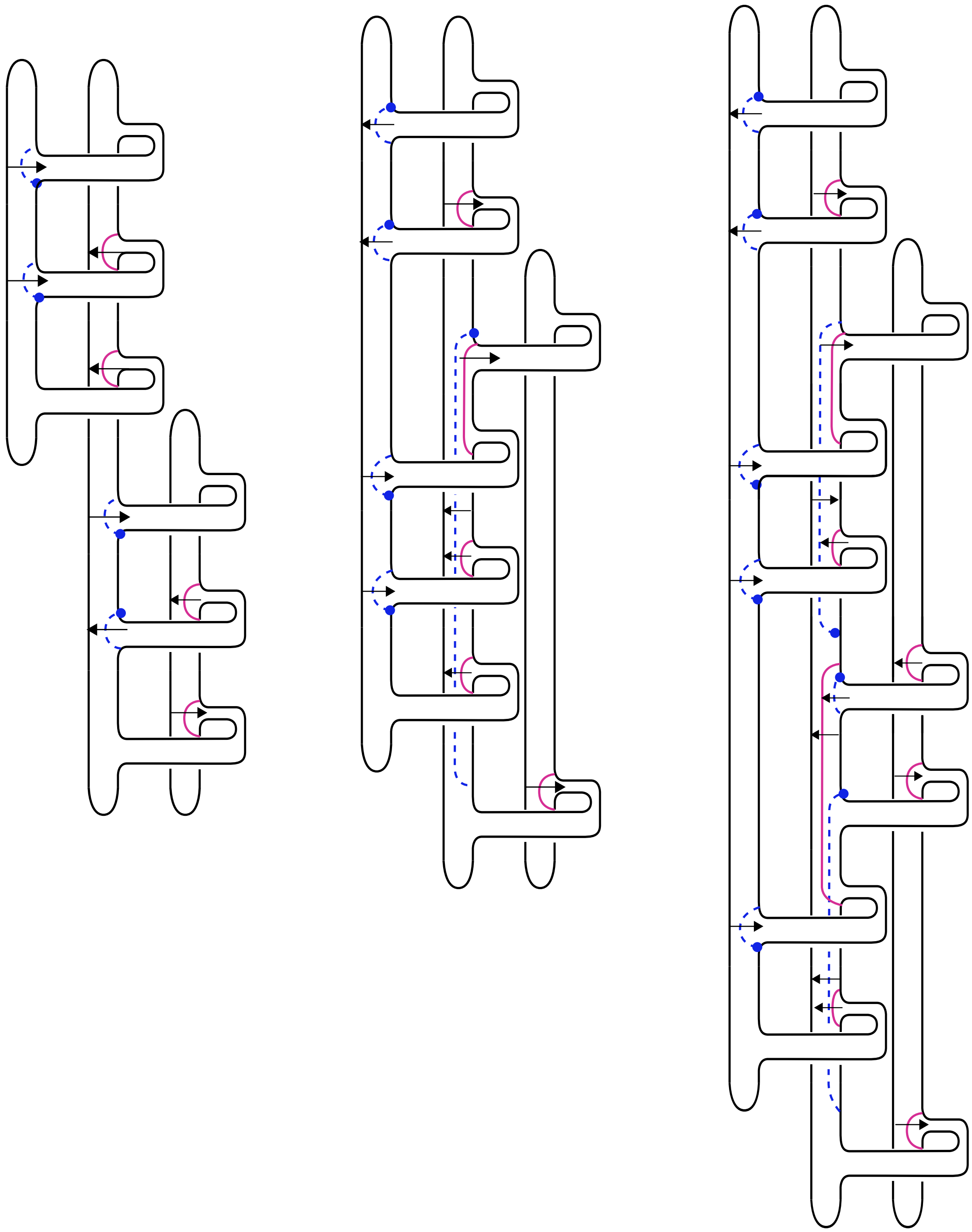

Figure 20: From left to right: laminar branched surfaces of Types A, B, and C.

Proposition 3.32. *(Building the branched surface for **Type B**)*

Suppose $\beta = \sigma_1^{a_1}\sigma_2\sigma_1^{a_2}\sigma_2,\ a_i \geq 2$ *and* $K = \hat{\beta}$. *There exists a sink-disk free branched* *surface $B \subset X_K$ with exactly one pair of linked arcs. Moreover, there is a sub-train-track τ' of τ carrying all rational slopes $r < 2g(K) - 1$.*

Proof. The spine of the branched surface is built from $F \times \{\frac{1}{2}\}$, fused with the product disks specified below:

$$\begin{aligned}
\beta &= \sigma_1^{a_1}\sigma_2\sigma_1^{a_2}\sigma_2 \\
&= \sigma_1^{a_1} \qquad \sigma_2 \quad \sigma_1^{a_2-1} \quad\; \sigma_1 \quad \sigma_2 \\
&= (\leftarrow)^{a_1}(\leftarrow)(\rightarrow)^{a_2-1}(\quad)(\quad)
\end{aligned} \tag{3.4}$$

Lemma 3.9 puts the product disks into standardized position. Cusping the disks as specified in (3.4) yields a branched surface, as in Figure 20. By Lemma 3.16, no product disk sector is a half sink disk. No disk sectors are half sink disks:

- $\widehat{\alpha}^-_{a_1+2}$ points out of the S_1 disk sector
- $\widehat{\alpha}^-_1$ points into the S_1 disk sector, so $\widehat{\alpha}^+_1$ points out of the S_2 disk sector
- $\widehat{\alpha}^-_{a_1+1}$ points into the S_2 disk sector, so $\widehat{\alpha}^+_{a_1+1}$ points out of the S_3 disk sector

Lemmas 3.25 and 3.26 guarantee no band sectors are sink disks. It remains to check the single polygon sector P, which lies in Seifert disk S_2. The boundary of P meets $\alpha^+_j, a_1 + 2 \leq j \leq c_1 + c_2 - 2, \alpha^-_{a_1+1}, \alpha^+_{a_1}$, and no other arcs $\alpha^\pm_j$. Since $\widehat{\alpha}^-_{a_1+1}$ points out of P, it is not a half sink disk. Thus, our branched surface B is sink disk free.

We are fusing c_1+c_2-2 product disks to $F \times \{\frac{1}{2}\}$, so there exists a sub-train-track τ' with c_1+c_2-2 sectors. By Lemmas 3.27 and 3.28, $\alpha^-_{a_1}$ and $\alpha^-_{a_1+1}$ are the unique pair of linked arcs. Thus τ' carries all slopes in $[0, c_1 + c_2 - 3) = [0, 2g(K) - 1)$. Including both sectors induced by α_{a_1+1} to τ' ensures that τ' carries all slopes $r < 2g(K)-1$. $\square$

The most nuanced construction arises in **Case C**:

Proposition 3.33. *(Building the branched surface for **Case C**)*
*Let $K = \hat{\beta}$, where β is of **Case C** (see Definition 3.29). There exists a sink-disk free branched surface $B \subset X_K$ with a unique pair of linked arcs. Moreover, there is a sub-train-track τ' of τ carrying all rational slopes $r < 2g(K) - 1$.*

Proof. The spine of the branched surface is built from $F \times \{\frac{1}{2}\}$, fused with the product disks specified by:

$$\begin{aligned}\beta &= \sigma_1^{a_1}\sigma_2^{b_1}\sigma_1^{a_2}\sigma_2^{b_2}\dots\sigma_1^{a_k}\sigma_2^{b_k}\\ &= \sigma_1^{a_1}\quad(\sigma_2)\ (\sigma_2^{b_1-1})\quad\sigma_1^{a_2}\quad\sigma_2^{b_2}\quad\sigma_1^{a_3}\quad\sigma_2^{b_3}\quad\dots(\sigma_1^{a_k-1})(\sigma_1)(\sigma_2^{b_k-1})(\sigma_2)\\ &= (\leftarrow)^{a_1}(\rightarrow)(\leftarrow)^{b_1-1}(\rightarrow)^{a_2}(\leftarrow)^{b_2}(\rightarrow)^{a_3}(\leftarrow)^{b_3}\dots(\rightarrow)^{a_k-1}(\quad)(\leftarrow)^{b_k-1}(\quad)\end{aligned} \tag{3.5}$$

Applying Lemma 3.9 puts the product disks into standardized position. Cusping the disks as specified in (3.5) yields a branched surface B. See Figure 20 for an example.

We check for half sink disks: by Lemma 3.16, no product disk sector is a half sink disk. No disk sector is a half sink disk:

- $\widehat{\alpha}^-_{a_1+b_1+1}$ points out of the S_1 disk sector
- $\widehat{\alpha}^-_1$ points into the S_1 disk sector, $\widehat{\sigma}^+_1$ points out of the S_2 disk sector
- whether $k = 2$ or $k = 3$, there exists a σ_2 letter in β cusped via $(\leftarrow)$. The corresponding image arc will point out of the S_3 disk sector

Lemmas 3.25 and 3.26 guarantee no band sectors are sink disks.

It remains to analyze polygon sectors. Unlike the cases analyzed in Propositions 3.30 and 3.32, there may be intersection points between α^+ and α^- arcs. Each intersection point will occur between consecutive blocks. Moreover, each intersection point indicates the existence of two polygon sectors. Reading from top-to-bottom, we number the intersection points $i_1, \dots, i_m, \dots i_n$. We note that n is bounded above by $k-1$, where k is the total number of blocks in β. Moreover, $n = k-1$ if and only if for every t, $b_t \geq 2$. In particular, the intersection point i_m does *not* have to occur between the blocks m and $m+1$. For example, in the rightmost diagram in Figure 20, the unique intersection point $i = i_1$ occurs between blocks 2 and 3.

As an intersection point indicates the existence of a pair of polygon sectors, we will identify the individual polygon sectors by their relative position. The polygon sectors associated to the intersection point i_m are labelled $P_{u,m}$ and $P_{\ell,m}$, and called *upper polygon* and *lower polygon* sectors respectively.

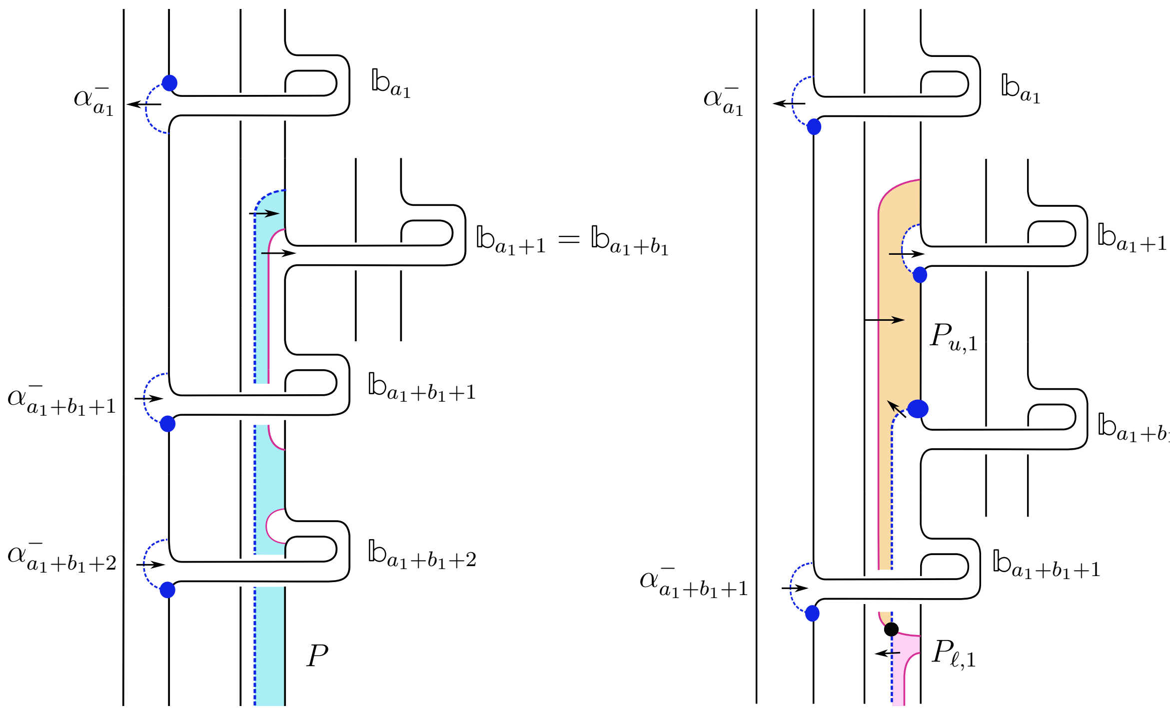

Figure 21: Studying b_1. On the left, we have $b_1 = 1$. The shaded region is the single polygon sector P, which is not a sink disk, as $\widehat{\alpha}^+_{a_1}$ points out of it. On the right, an example with $b_1 = 2$. The upper and lower polygon sectors, $P_{u,1}$ and $P_{\ell,1}$, are shaded; these polygon sectors meet at the point i_1 (not labelled, but indicated in the diagram). $P_{u,1}$ is not a sink disk because $\widehat{\alpha}^-_{a_1+1}$ points out of it. $P_{\ell,1}$ is not a sink disk because $\widehat{\alpha}^-_{a_1+b_1}$ points out of it.

We first analyze the behavior of b_1. If $b_1 = 1$, then we have a single polygon sector P. It is not a half sink disk, as $\widehat{\alpha}^+_{a_1}$ points out of the region; see (Figure 21, left). If $b_1 \geq 2$, we have a pair of polygon sectors to analyze; see (Figure 21, right):

- The boundary of $P_{u,1}$ meets the arcs
  - $\alpha^-_j, a_1 + 1 \leq j \leq a_1 + b_1$
  - $\alpha^+_{a_1}$,
- The boundary of $P_{\ell,1}$ meets the arcs
  - $\alpha^-_{a_1+b_1}$,
  - $\alpha^+_{a_1}$,
  - $\alpha^+_j, a_1 + b_1 + 1 \leq j \leq a_1 + b_1 + a_2 - 1$,

Since $\widehat{\alpha}^-_{a_1+1}$ points out of $P_{u,1}$, and $\widehat{\alpha}^-_{a_1+b_1}$ points out of $P_{\ell,1}$, neither are half sink disks.

We now analyze the remaining polygon sectors. If, for $q \geq 2$, the q^{th} block has $b_q = 1$, there will be a single polygon region. It is not a half sink disk because $\widehat{\alpha}^-_{a_1+b_1+\ldots+a_q}$ points out of it region (see Figure 22, left). If $b_q \geq 2$, then the polygon sectors come in pairs; all such pairs can be analyzed simultaneously (see Figure 22, right). Suppose i_m is the intersection point between $P_{u,m}$ and $P_{\ell,m}$, which occur at the transition from block t to block $t+1$. For the pair $P_{u,m}$ and $P_{\ell,m}$:

- the boundary of $P_{u,m}$ meets the arcs
  - α^-_j, where $a_1 + b_1 + \ldots a_t + 1 \leq j \leq a_1 + b_1 + \ldots + a_t + b_t$
  - $\alpha^+_{a_1+b_1+\ldots+a_t}$
- the boundary of $P_{\ell,m}$ meets the arcs
  - $\alpha^-_{a_1+b_1+\ldots+a_t+b_t}$
  - $\alpha^+_{a_1+b_1+\ldots+a_t}$
  - α^+_j, where $a_1 + b_1 + \ldots + b_t + 1 \leq j \leq a_1 + b_1 + \ldots + b_t + a_{t+1} - 1$

For each $2 \leq m \leq n$, $P_{u,m}$ is not a sink disk: $\widehat{\alpha}^+_{a_1+b_1+\ldots+a_t}$ points out of it. Furthermore, $P_{\ell,m}$ has $\widehat{\alpha}^-_{a_1+b_1+\ldots+a_t+b_t}$ pointing out of it. Thus B is sink disk free.

We cusped $(c_1-1)+(c_2-1)$ arcs. By Lemma 3.27, there exists a single linked pair, arising from the arcs associated to the first two occurrences of σ_2 in β. Thus, there exists a sub-train-track τ' carrying all slopes in $[0, c_1+c_2-3) = [0, 2g(K)-1)$. Including the sectors induced by α_{a_1+1} to τ' ensures that τ' carries all rational $r < 2g(K)-1$. □

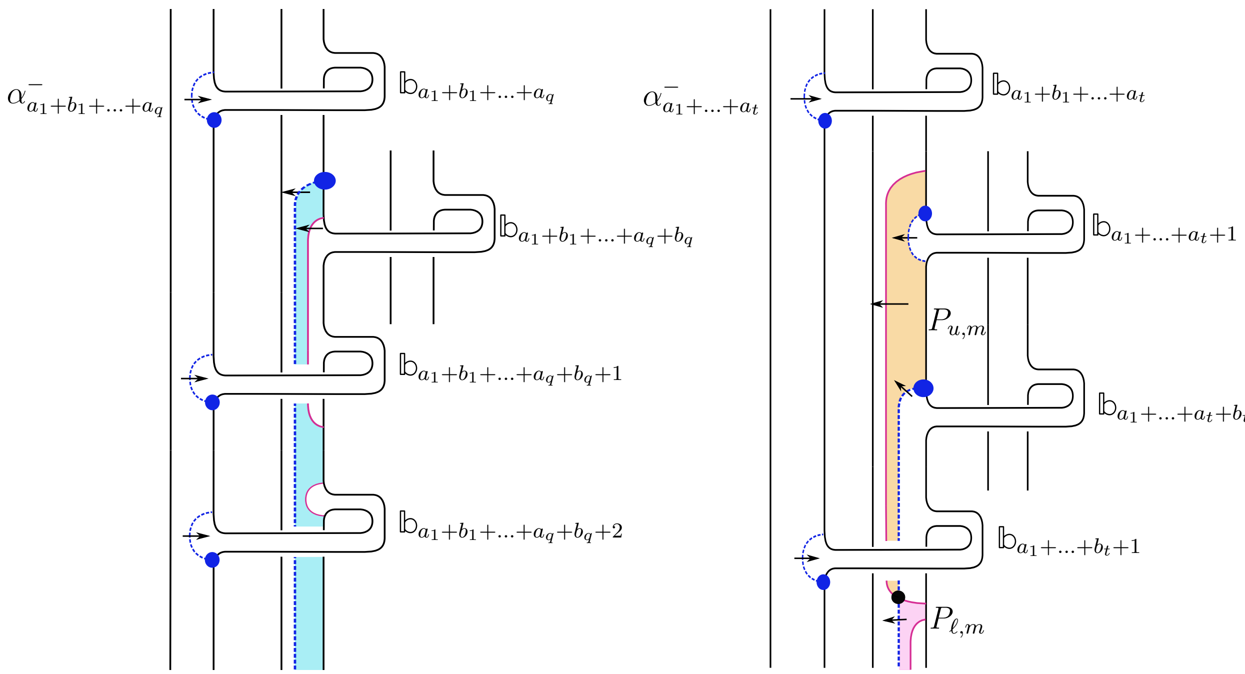

Figure 22: On the left: we have $b_q = 1$. The shaded region is the single polygon sector, which is not a sink disk because $\widehat{\alpha}^+_{a_1+b_1+\ldots+a_q}$ points out of it. On the right: an example with $b_m = 2$. The upper and lower polygon sectors, $P_{u,m}$ and $P_{\ell,m}$, are shaded; they meet at the point i_m (not labelled, but indicated in the diagram). $P_{u,m}$ is not a sink disk because $\widehat{\alpha}^+_{a_1+\ldots+a_t}$ points out of it. $P_{\ell,m}$ is not a sink disk because $\widehat{\alpha}^-_{a_1+\ldots+a_t+b_t}$ points out of it.

3.3.3 Finale

We conclude this section with the proof of the main theorem.

Proof of Theorem 1.15. Let $K \subset S^3$ be the closure of a positive 3-braid β. After isotopy, β has the form specified by Equation 3.1, and by Definition 3.29 is Type A, B or C. By Propositions 3.30, 3.32, 3.33, there exists a branched surface $B \subset X_K$ inducing a sub-train-track τ' carrying all rational slopes in the interval $(-\infty,\ 2g(K)-1)$. B is laminar Proposition 3.17 (we note that if β is Type A, then we additionally apply Remark 3.31). Applying Theorem 2.4 yields a family of essential laminations $\{\mathcal{L}_r \mid r \in (-\infty, 2g(K)-1) \cap \mathbb{Q}\}$, where $\mathcal{L}_r$ meets ∂X_K in simple closed curves of slope r. Proposition 3.24 extends the essential lamination $\mathcal{L}_r$ to a taut foliation $\mathcal{F}_r$ in X_K, foliating ∂X_K by simple closed curves of slope r. Performing r-framed Dehn filling yields $S^3_r(K)$ endowed with a taut foliation. □

Chapter 4

1–bridge braids

4.1 Preliminaries

We generalize the techniques developed in Chapter 3 to produce taut foliations in 1-bridge braid exteriors. Gabai defines a 1-bridge braid $K(w, b, t)$ in $D^2 \times S^1$ to be a knot, realized as the closure of a positive braid β, which is specified by three parameters: w, the braid index; b, the bridge width; and t, the twist number: $\beta = (\sigma_b\sigma_{b-1}\ldots\sigma_2\sigma_1)(\sigma_{w-1}\sigma_{w-2}\ldots\sigma_2\sigma_1)^t$ where $1 \leq b \leq w-2,\ 1 \leq t \leq w-2$ [Gab90]. We consider a slightly more general definition:

Definition 4.1. *A (positive) 1-bridge braid K in S^3 is a knot realized as the closure of a braid β on w-strands, where*

$$\beta = \underbrace{(\sigma_b\sigma_{b-1}\ldots\sigma_2\sigma_1)}_{\text{bridge subword}}(\sigma_{w-1}\sigma_{w-2}\ldots\sigma_2\sigma_1)^t$$

*for $w \geq 3,\ 1 \leq b \leq w-2,\ t \geq 1$. We call the first b letters of β the **bridge subword**.*

In particular, we allow a 1-bridge braid in S^3 to have arbitrarily large twist number.

Remark 4.2. *There are no 1-bridge braids with $w = 3$; we may assume $w \geq 4$.*

Theorem 1.20. *Let K be a (positive) 1-bridge braid in S^3. Then for every $r \in (-\infty, g(K)) \cap \mathbb{Q}$, the knot exterior $X_K := S^3 - \mathring{\nu}(K)$ admits taut foliations meeting the boundary torus T in parallel simple closed curves of slope r. Moreover, the manifold obtained by r-framed Dehn filling, $S^3_r(K)$, admits a taut foliation.*

Every 1-bridge braid K is a fibered knot in S^3. As in Theorem 1.15, proving Theorem 1.20 requires building a laminar branched surface B from a copy of the fiber surface F and a collection of product disks.

4.2 Branched surfaces for 1–bridge braids

Definition 4.3. *Let $\mathcal{B}_w$ denote the braid group on w strands. Suppose $\beta' \in \mathcal{B}_w$ such that $\beta' = \sigma_m\sigma_{m-1}\sigma_{m-2}\ldots\sigma_2\sigma_1$, with $1 \leq m \leq w-1$. We call the canonical fiber surface F' for β', built from w disks and m 1-handles, a* ***horizontal slice****.*

We can view the canonical fiber surface F for a 1-bridge braid $K(w, b, t)$ as built by vertically stacking $t+1$ horizontal slices, $\mathbb{h}_0, \mathbb{h}_1, \ldots, \mathbb{h}_{t+1}$: numbering the horizontal slices from top-to-bottom, the horizontal slice $\mathbb{h}_0$ comes from the bridge subword; the remaining t horizontal slices $\mathbb{h}_1, \ldots \mathbb{h}_t$ come from the t occurrences of the subword $\sigma_{w-1}\sigma_{w-2}\ldots\sigma_2\sigma_1$ in β; see (Figure 23, upper) for an example.

Definition 4.4. *A Seifert disk S_i is* ***odd (even)*** *if i is odd (even).*

As in Sections 3.2 and 3.3, we provide cusping directions alongside β. That is, given a 1-bridge braid K with braid word presented as in Definition 4.1, we will choose disjoint product disks as in Section 3.2.1. The boundaries of these disks will lie entirely in consecutive Seifert disks and consecutive bands of the same type; see (Figure 23, upper). As in Definition 3.15 (with the paragraph preceding it) and Section 3.3, the data of the disks and their co-orientations are recorded in tandem with the braid word; see (Figure 23, lower) for example of a portion of the resulting branched surface.

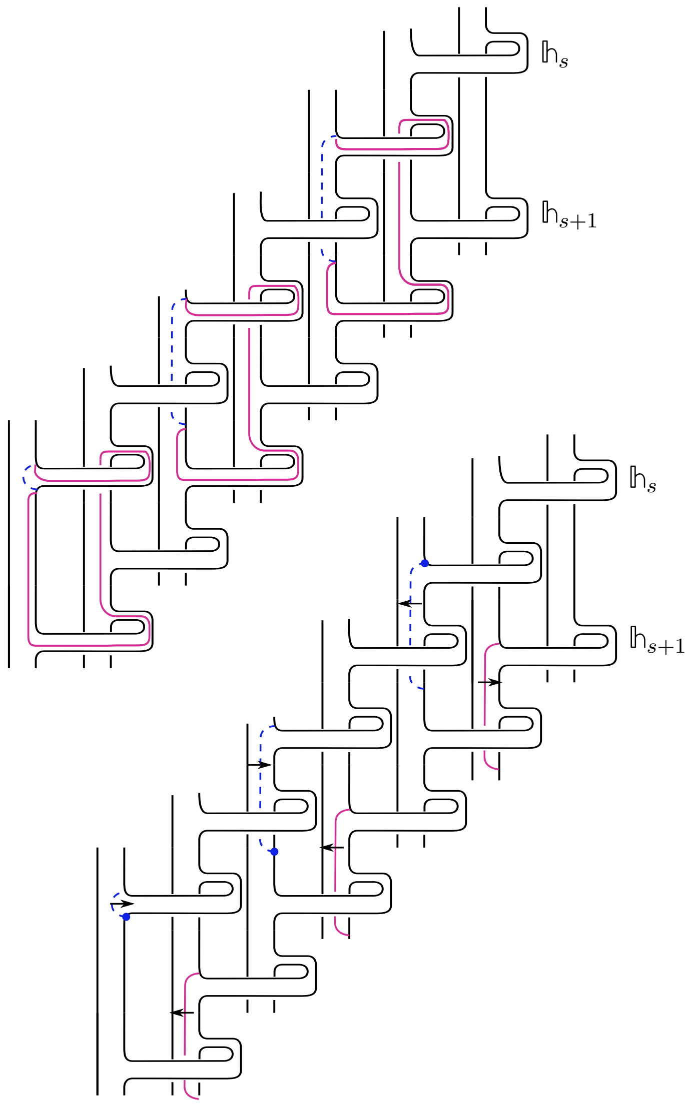

Figure 23: Upper: the consecutive horizontal slices $\mathbb{h}_s$ and $\mathbb{h}_{s+1}$ of a 1-bridge braid fiber surface. As in Figure 9, we have identified three product disks, by indicating where the disks meet $F^- \cup F^+$. The disks look like those in Figure 4. Lower: we first performed a spinal isotopy so that the α^+ arcs lie only in Seifert disks, and then co–oriented the disks as shown. The result is a portion of a branched surface.

Proposition 4.5. *For K a 1-bridge braid in S^3, the following cusping directions specify a sink disk free branched surface:*

- *σ_i is cusped via ( ) $\iff$ i is even, or i is odd and σ_i is associated to a 1-handle used to build $\mathbb{h}_t$.*
- *Otherwise, σ_i is cusped via $(\leftarrow)$ or $(\rightarrow)$, as specified below:*
    - *The first occurrence of σ_i in β is cusped $(\leftarrow)$.*
    - *All other occurrences of σ_i in β are cusped via $(\rightarrow)$.*

Proof. Following Sections 3.2 and 3.3, the directions above specify arcs α_j^-; applying the monodromy to these arcs produces the product disks $\{D_j\}$. Build the spine for a branched surface from $F \times \{\frac{1}{2}\}$ and $\{D_j\}$. Applying the proof of Lemma 3.9 splits the spine of B, putting the disks in standard position. After standardizing, all α_j^- lie in odd Seifert disks S_i, and all α_j^+ lie in even Seifert disks. Choosing co-orientations for $\{D_j\}$ as specified by the instructions provided yields a branched surface B. See Figure 24 for an example of such a branched surface.

We check B has no sink disks. No Seifert disk S_i contains both α_j^- and α_ℓ^+ arcs, thus there are no polygon sectors. It suffices to check that no disk and band sectors are sink disks. There are at most $t+1$ band sectors: one for each horizontal slice $\mathbb{h}_0, \mathbb{h}_1, \dots, \mathbb{h}_t$.

Definition 4.6. *The branch sector containing the bands in $\mathbb{h}_i$ is the i^{th}* ***band sector****, and denoted $\mathbb{B}_i$.*

We consider 3 cases: $t = 1$, $t = 2$, and $t \geq 3$.

If $t = 1$, then after destabilizing, $K = K(w, b, 1) \approx T(b+1, 2) \approx T(2, b+1)$ as knots in S^3. In Proposition 3.30, we constructed a laminar branched surface B for any knot $K = T(2, n)$, where the induced train track τ carried all slopes $(-\infty, 2g(K)-1)$.

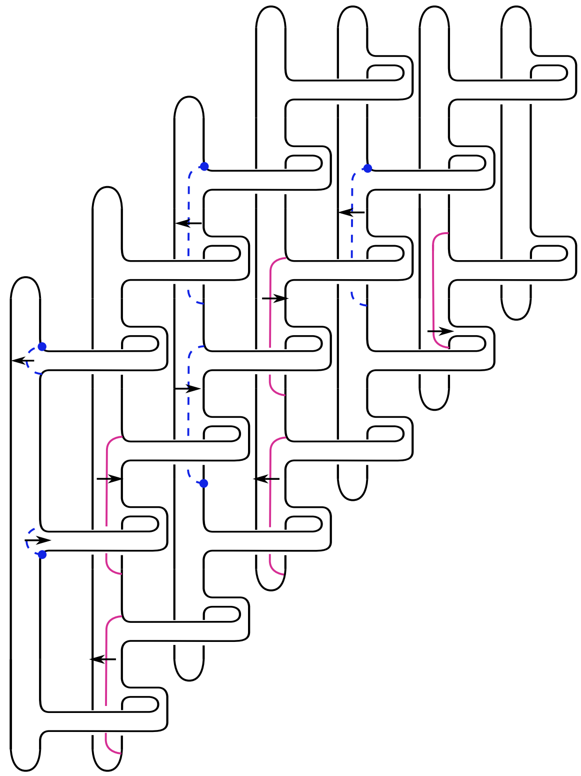

Figure 24: A laminar branched surface for the 1-bridge braid $K(7, 4, 2)$

Appealing to Theorem 1.15 yields a stronger result than the one we seek for Theorem 1.20.

Before treating the $t = 2$ and $t \geq 3$ cases, we prove:

Lemma 4.7. *Let B be the branch surface described above, for $K(w, b, t)$ with $t \geq 2$. If b is odd (resp. even), the disk sectors $S_1, \ldots S_{b+1}$ (resp. $S_1, \ldots S_b$) are not half sink disks.*

Proof. If b is odd (resp. even), then every odd Seifert disk among $S_1, \ldots, S_b$ (resp. $S_1, \ldots, S_{b-1}$) contains arcs α_j^- cusped via both ($\leftarrow$) and ($\rightarrow$) (this is guarenteed since $t \geq 2$). Lemma 3.13 guarantees all Seifert disks $S_1, S_2, \ldots, S_{b+1}$ (resp. $S_1, S_2, \ldots, S_b$) contain arcs cusped via both ($\leftarrow$) and ($\rightarrow$). Each of these disks contains an outward pointing cusped arc, hence they are not half sink disks. This completes the proof of Lemma 4.7.

We return to the proof of Proposition 4.5.

If $t = 2$, we have a three subcases:

- $b = w - 2$, $b \equiv w \equiv 0 \mod 2$

  No band sectors are half sink disks: $\widehat{\alpha}_b^-$, $\widehat{\alpha}_{b+1}^-$, and $\widehat{\alpha}_{b+w-1}^+$ point out $\mathbb{B}_0, \mathbb{B}_1$ and $\mathbb{B}_2$ respectively.

  By Lemma 4.7, the disk sectors $S_1, S_2, \ldots, S_{w-2}$ are not half sink disks. S_{w-1}, S_{w-2}, and $\mathbb{B}_1$ are part of the same branch sector; we already determined $\mathbb{B}_1$ is not a half sink disk. Finally, $\widehat{\alpha}_{b+1}^+$ points out of S_w, and B is sink disk free.

- $b = w - 2$, $b \equiv w \equiv 1 \mod 2$

  No band sectors are half sink disks: $\widehat{\alpha}_b^-$ and $\widehat{\alpha}_{b+w-1}^+$ point out of $\mathbb{B}_0$ and $\mathbb{B}_2$ respectively. $\mathbb{B}_1$ and $\mathbb{B}_2$ are in the same branch sector, so $\mathbb{B}_2$ is not a half sink disk.

  By Lemma 4.7, the Seifert disks $S_1, S_2, \ldots, S_{w-1}$ are not half sink disks. S_w and $\mathbb{B}_2$ are in the same branch sector. B is sink disk free.

- $b < w - 2$

  $\widehat{\alpha}_b^-$ and $\widehat{\alpha}_{b+w-1}^+$ point out of $\mathbb{B}_0$ and $\mathbb{B}_2$ respectively. Either $\widehat{\alpha}_{b+1}^-$ (if $w \equiv 0 \mod 2$) or $\widehat{\alpha}_{b+2}^-$ (if $w \equiv 1 \mod 2$) points out of $\mathbb{B}_1$. No band sectors are half sink disks.

  If $b \equiv 0 \mod 2$, then by Lemma 4.7, $S_1, S_2, \ldots, S_b$ are not half sink disks. Every even Seifert disk S_i with $i \geq b+2$ contains an image arc cusped via $(\rightarrow)$. S_{b+1} is in the same branch sector as S_1. All other Seifert disks $S_i, i \geq b+3$ are in the same branch sector as $\mathbb{B}_1$, which we know has an outwardly cusped arc. B is sink disk free.

Alternatively, if $b \equiv 1 \mod 2$, then by Lemma 4.7, $S_1, S_2, \ldots, S_{b+1}$ are not half sink disks. Every even Seifert disk $S_i, i \geq b+3$ contains an image arc cusped via $(\rightarrow)$. Every odd Seifert disk $S_i, i \geq b+2$ is in the same branch sector as S_1. B is sink disk free.

Consider a 1-bridge braid with $t \geq 3$. Every odd Seifert disk S_i contains arcs cusped via both $(\leftarrow)$ and $(\rightarrow)$. If w is even (resp. odd), the proof of Lemma 4.7 guarantees $S_1, \ldots, S_w$ (resp. $S_1, S_2, \ldots, S_{w-1}$) are not half sink disks. If w is odd, S_1 and S_w will be in the same disk sector. We conclude no disks sectors are half sink disks.

Finally, we verify no band sectors are sink disks: $\widehat{\alpha}_b^-$ points out of $\mathbb{B}_0$. For each $2 \leq i \leq t$, $\widehat{\alpha}_{b+(i-1)(w-1)}^-$ points out of $\mathbb{B}_i$. We need only confirm $\mathbb{B}_1$ is not a half sink disk. If $b < w-2$, $\widehat{\alpha}_{b+2}^-$ points out of $\mathbb{B}_1$ (if w is odd) or $\widehat{\alpha}_{b+1}^-$ does (if w is even). If $b = w-2$ and $w \equiv 1 \mod 2$, then $\mathbb{B}_1$ and S_w are in the same branch sector; we know $\mathbb{B}_1$ is not a half sink disk. If $b = w-2$ and $w \equiv 0 \mod 2$, then $\widehat{\alpha}_{b+1}^-$ points out of $\mathbb{B}_1$. We conclude B is sink disk free. □

Lemma 4.8. *The train track τ, induced by B, admits no linked pairs of arcs.*

Proof. All arcs α_j^- contributing maximally to τ lie in odd Seifert disks S_i. Therefore, the only way to produce a linked pair of arcs is if σ_m^- and σ_{m+w-1}^- are cusped via $(\rightarrow)$ and $(\leftarrow)$ respectively, as in Figure 25. Our cusping directions avoid these instructions. □

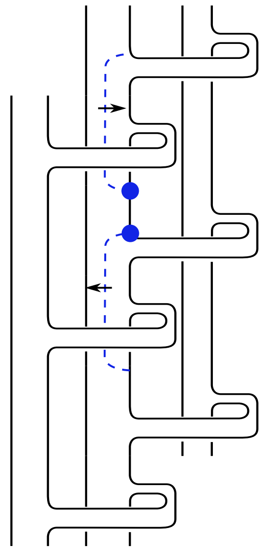

Figure 25: These cusping instructions for α_m^- and α_{m+w-1}^- yield a linked pair.

Definition 4.9. *Let K be a 1-bridge braid, and B the sink disk free branched surface built in Proposition 4.5. Define Γ to be the number of product disks used to build B.*

Lemma 4.10. *The induced train track τ carries all rational slopes in $(-\infty, g(K))$.*

Proof. By Lemma 4.8, we have no linked arcs; therefore, we need only count the total number of product disks Γ used to build B, and verify $\Gamma \geq g(K)$. It is straightforward to compute the genus of any 1-bridge braid K:

$$\chi(F) = w - ((w-1)t + b) \implies g(K) = \frac{-\chi(F)+1}{2} = \frac{wt - w - t + b + 1}{2}$$

The value of Γ depends on the parity of w and b; we analyze the 4 possible cases in Table 1 below. In each case, $\Gamma \geq g(K)$. Including both sectors of τ induced by α_b yields a sub-train track τ' carrying all slopes in $(-\infty, g(K))$. Therefore, for any K, the train track τ induced by the branched surface B carries all rational slopes $r < g(K)$. □

parity of w	parity of b	Γ
even	even	$\frac{(t-1)w}{2}+\frac{b}{2}=\frac{wt+b-w}{2}$
even	odd	$\frac{(t-1)w}{2}+\frac{b+1}{2}=\frac{wt-w+b+1}{2}$
odd	even	$\frac{(w-1)(t-1)}{2}+\frac{b}{2}=\frac{wt-w-t+b+1}{2}$
odd	odd	$\frac{(w-1)(t-1)}{2}+\frac{b+1}{2}=\frac{wt-w-t+b+2}{2}$

Table 1: The slopes carried by the train track of a 1–bridge braid branched surface.

4.3 Proving the 1–bridge braids theorem

Proof of Theorem 1.20. By Proposition 4.5, for any 1-bridge braid $K \subset S^3$, there exists a sink disk free branched surface $B \subset X_K$. We want to prove that B is laminar by applying Proposition 3.17. However, we need to modify the proof of said proposition to show that B cannot fully carry an annulus (our proof of (3) in Proposition 3.17 relied on a local model that does not apply to 1-bridge braids).

This is straightforward. The cusping directions provided in Proposition 4.5 focuses our attention to the first Seifert disk; see Figure 26. Let the weights of the disk sectors

S_1 and S_2 be w_1 and w_2 respectively, the weight for the horizontal slice $\mathbb{h}_1$ is w_3, and the weight of the isotoped product disks associated to the first two occurrences of α_1 are w_4 and w_5 respectively. The switch relations for a branched surface to carry a compact surface imply the following:

$$w_1 = w_2 + w_4 \qquad w_3 = w_1 + w_5 \qquad w_3 = w_2 + w_4$$

This implies that $w_3 = w_1$, thus $w_5 = 0$. This contradicts that S is fully carried by B. We conclude that B cannot carry any compact surface, and therefore does not carry an annulus. Thus, B is laminar.

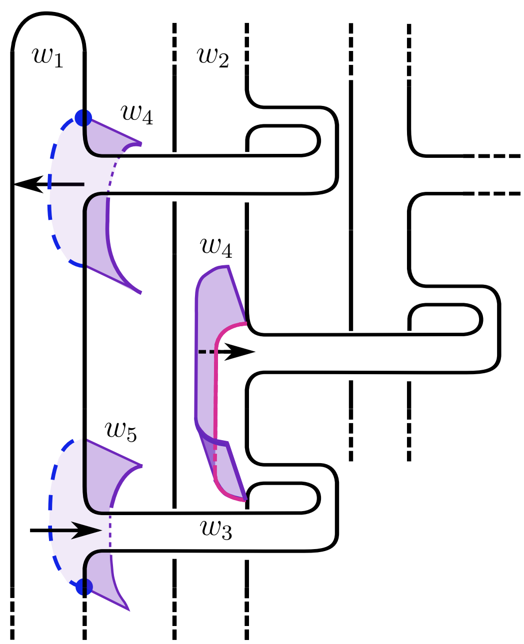

Figure 26: A local picture of the branched surface near the first Seifert disk S_1. For simplicity, the first product disk appears broken in our figure; it has weight w_4. We do not see all of the second product disk, which has weight w_5. The standard switch relations induced by the branch loci indicate that $w_5 = 0$. Thus B cannot carry a compact surface.

By Lemma 4.10, the boundary train track τ carries all rational slopes $r < g(K)$. Applying Theorem 2.4 yields a family of essential laminations $\mathcal{L}_r$ carried by B, where $r < g(K)$. Proposition 3.24 extends each essential lamination $\mathcal{L}_r$ to a taut foliation $\mathcal{F}_r$ meeting ∂X_K in simple closed curves of slope r. Performing r-framed Dehn filling produces $S^3_r(K)$ endowed with a taut foliation. $\square$

Chapter 5

Positive n–braids

In this chapter, we partially generalize Theorem 1.15 to the class of all positive braid knots of any braid index n. In particular, we prove:

Theorem 1.21. *Suppose K is a knot in S^3 which can be realized as the closure of a positive braid. Then for all $r \in (\infty, g(K)-1)$, $S^3_r(K)$ admits a taut foliation.*

In [DRa], Delman–Roberts proved that if K is a composite fibered knot, then for all $r \in \mathbb{Q}$, $S^3_r(K)$ admits a taut foliation. Therefore, to prove Theorem 1.21, it suffices to restrict to the class of positive braids on $n \geq 4$ strands whose closures are prime knots. Indeed, Theorem 1.21 is a corollary of the following theorem:

Theorem 5.1. *Suppose K is a prime knot in S^3 which can be realized as the closure of a positive braid on $n \geq 4$ strands. Then for all $r \in (\infty, g(K)-1)$, $S^3_r(K)$ admits a taut foliation.*

Remark 5.2. *As stated in Section 1.2, our proof of Theorem 5.1 requires dividing such positive braids into four categories; in doing so, we actually construct taut foliations in $S^3_r(K)$ for all $r \in (-\infty, g(K))$ in all but one case.*

This chapter is dedicated to proving Theorem 5.1.

5.1 The construction and an example

In this section, we demonstrate the construction alongside an example. In addition to establishing some preliminaries, the example demonstrates the strategy for proving Theorem 5.1 for a generic positive braid (our definition of "generic" will become clear in Section 5.2). Throughout this section, we use the braid defined in (2.1), reproduced here for convenience:

$$\beta \approx \sigma_1\sigma_3\sigma_2\sigma_3\sigma_4\sigma_1^2\sigma_3\sigma_2\sigma_3\sigma_4\sigma_3$$

In particular, we will use the plumbing structure of Section 2.3, and the explicit factorization of the monodromy, to choose arcs on the fiber surface F. We outline the construction of taut foliations in $S^3_r(K)$, K realized as the closure of a positive braid on n strands, where $r \in (-\infty, g(K))$ and $n \geq 4$:

Section 5.1.2: Design a template for a branched surface for a column of the braid.

Section 5.1.3: Apply the template to multiple columns to build a branched surface B.

Section 5.1.4: Show that B is laminar.

Section 5.1.5: Calculate the slopes carried by the train track τ_B.

Section 5.1.6: Construct taut foliations in the surgered manifolds.

But first, we establish some necessary preliminaries about positive braid words.

5.1.1 Preliminaries about β

First, we recall Definition 2.11:

Definition 2.11 *The i^{th}* ***column of*** *F, denoted Γ_i, is the union of the Seifert disks S_i, S_{i+1}, and the bands $\mathbb{b}_1, \dots \mathbb{b}_{c_i}$ connecting them.*

Definition 5.3. *Let c_i denote the number of σ_i that appear in β. We define $\mathcal{C}_{odd}$ (resp. $\mathcal{C}_{even}$) to be the sum of all c_i where i is odd (resp. even), and $\mathcal{C}$ is the total* *number of crossings in β.*

Note that $\mathcal{C}_{\text{odd}} + \mathcal{C}_{\text{even}} = \mathcal{C}$, which is also the length of the braid word. Since we are interested in braids whose closures are knots (and not links), we must have that $c_i \geq 1$ for all $1 \leq i \leq n-1$.

In fact, we can assume that for all i, $c_i \geq 2$. Suppose otherwise: if there exists some i such that $c_i = 1$, then we could destabilize the braid and decrease the braid index. This operation preserves positivity and the isotopy type of the closure as a link in S^3.

Definition 5.4. *For $1 \leq i \leq n-1$, define the functions $\mathcal{B}_i : \beta \to \mathbb{Z}^+$ as follows: conjugate β so it is of the form $\beta \approx \sigma_i^{p_1} w_1 \sigma_i^{p_2} w_2 \ldots \sigma_i^{p_k} w_k$, where for all $1 \leq j \leq k$, $1 \leq p_j$ and w_j is a subword of β with no σ_i letters. Then $\mathcal{B}_i(\beta) := k$.*

Indeed, the functions $\mathcal{B}_i$ are well–defined, as we are only applying braid conjugation (and not using the braid relations).

Lemma 5.5. *If $\widehat{\beta}$ is a prime knot, then for all $1 \leq i \leq n-1$, $\mathcal{B}_i(\beta) \geq 2$.*

Proof. We proceed via a proof by contrapositive: suppose there exists some i such that $\mathcal{B}_i(\beta) = 1$. Therefore, there exists some conjugation of β such that $\beta \approx \sigma_i^{p_1} w_1$, where w_1 is a word spelled without σ_i letters. But this means that β can be realized a connected sum of two braids β_1 and β_2; see Figure 27 for an example alongside the splitting S^2. $\square$

Going forwards, we assume that $\widehat{\beta}$ is prime.

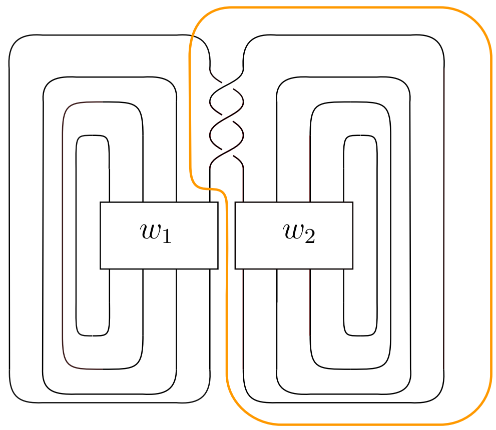

Figure 27: A braid with $\mathcal{B}_4(\beta) = 1$; w_1 and w_2 are braid words in the Artin generators σ_j with $j \neq 4$. The orange unknotted circle is the equator of an S^2 realizing $\widehat{\beta}$ as the connected sum of two knots.

5.1.2 Design a template for a branched surface for a column of the braid

To build the branched surface B for Theorem 1.21, we will design and apply a standard template to a subset of the columns of F. This requires three steps:

- Identifying the product disks in a column Γ_j
- Building the spine for a branched surface, supported in Γ_j
- Assign co–orientations to build the branched surface

Identify product disks in a column Γ_j

The construction in Lemma 2.9 not only identifies a factorization of the monodromy of the fiber surface for $\widehat{\beta}$, but it also identifies plumbing arcs for the Hopf bands. Thus, we can exactly identify the images of the plumbing arcs under the monodromy, as in Lemma 2.9.

To identify product disks in column Γ_j, we will first put β in some standard form with respect to σ_j:

Definition 5.6. *Fix some $1 \leq i \leq n-1$. Conjugate β so that $\beta \approx \sigma_i^{p_1} w_1 \sigma_i^{p_2} w_2 \dots \sigma_i^{p_k} w_k$ <u>and</u> w_1 contains a σ_{i+1} (resp. σ_{i-1}). Call the band $\mathbb{b}$ corresponding to the first σ_{i+1} (resp. σ_{i-1}) in w_1 a **right (resp. left) splinter**.*

Definition 5.7. *A positive braid β is **standardized with respect to** σ_i when β can written as:*

$$\beta \approx \sigma_i w_1 \sigma_i^{p_2} w_2 \dots \sigma_i^{p_k} w_k \sigma_i^{w_1 - 1} \approx \sigma_i w_1 \sigma_i^{p_2} w_2 \dots \sigma_i^{p_k} w_k'$$

such that (1) for all $1 \leq j \leq k$, w_j has no σ_i letters (so, $w_k' \approx w_k \sigma_i^{w_1 - 1}$), and (2) w_1 has a right splinter.

Lemma 5.8. *For every $1 \leq i \leq n-1$, β can be standardized with respect to σ_i.*

Proof. Fix some i as in the statement. Since β is prime, then Lemma 5.5 implies that $\mathcal{B}_i(\beta) \geq 2$. Since $c_i \geq 2$, there exists some j for which the subword w_j contains a σ_{i+1} letter. Conjugate β so this subword becomes w_1. □

Note: these standardized forms of β are not well–defined; our construction is independent of well–definedness.

So, assume β is standardized with respect to σ_j. The construction of Section 2.3 thereby specifies $c_j - 1$ plumbings in column Γ_j. We will choose the product disks obtained by applying the monodromy to the $c_j - 1$ plumbing arcs. In particular, we get $c_j - 1$ disks, all sitting in column Γ_j.

The spine for a branched surface in a column Γ

Now that we have identified the product disks in column Γ_j, we can build the spine for a branched surface. The branch locus is supported in Seifert disks S_j, S_{j+1}, and the bands connecting them.

Definition 5.9. *The spine $\mathbb{S}_j$ is formed by fusing the fiber surface F with the product disks $\{\mathbb{D}_{j_t} \mid 1 \leq t \leq c_j - 1\}$ in column Γ_j.*

As in Chapters 3 and 4, we will now simplify the spine $\mathbb{S}_j$ via a spinal isotopy (see Definition 3.7).

Definition 5.10. *Let $\mathcal{A}_j$ denote the collection of plumbing arcs in Seifert disk S_j.*

As a result of the spinal isotopy, on F, we see geodesic representatives of both the plumbing arcs, $\alpha \in \mathcal{A}_j$, and their images, $\varphi(\alpha)$, as elements in $H_1(F, \partial F)$. Mildly abusing notation, we will refer to the spine after the spinal isotopy as $\mathbb{S}_i$, and note that the branch locus is now supported in S_j and S_{j+1}.

Co–orient the product disks

The previous section specifies how to build a spine for a branched surface in a column of the braid. To produce a branched surface, we need to specify co–orientations for the product disks. We recall an essential part of Definition 3.15, where we described how to provide cusp directions in tandem with a braid word.

Definition 5.11. *An arc $\alpha^{\pm}$ on $F^{\pm}$ is co–oriented **to the left (resp. right)** if, when looking at the fiber surface F, the arc is decorated with a left (resp. right) pointing arrow, indicating the smooth direction of the locus of where the product disk meets the fiber surface.*

We are now ready to assign co–orientations to the (isotoped) product disks; with β standardized with respect to σ_j, smooth the plumbing arcs $\mathcal{A}_j \subset S_j$ as follows:

- smooth the first plumbing arc to the left
- smooth all subsequent plumbing arcs to the right

This concludes the description of the template for a branched surface B_j, whose branch locus is supported in the adjacent Seifert disks S_j and S_{j+1}.

5.1.3 Apply the template to multiple columns

In the previous section, we designed a template which we can apply to a column of the fiber surface. We will choose multiple columns in F, and apply the template to these columns, one–by–one. We study the distribution of crossings across the odd and even columns to choose the plumbing arcs, and therefore the product disks, to include in our branched surface B.

Definition 5.12. *Let* $\mathcal{C}_{\text{big}} = \max\{\mathcal{C}_{\text{odd}},\ \mathcal{C}_{\text{even}}\}$*. If* $\mathcal{C}_{odd} = \mathcal{C}_{even}$*, then set* $\mathcal{C}_{big} = \mathcal{C}_{odd}$*.*

If $\mathcal{C}_{\text{big}} = \mathcal{C}_{\text{odd}}$ (resp. $\mathcal{C}_{\text{even}}$), then we will apply our template to the "odd (resp. even) columns", i.e. the columns Γ_j where j is odd (resp. even). We do this in stages, one column at a time.

Definition 5.13. *Let* Γ_f *denote the first column of the braid to which the template is applied.*

If $\mathcal{C}_{\text{big}} = \mathcal{C}_{\text{odd}}$, then $\Gamma_f = \Gamma_1$; otherwise, if $\mathcal{C}_{\text{big}} = \mathcal{C}_{\text{even}}$, then $\Gamma_f = \Gamma_2$. As in Section 5.1.2, we: conjugate β to be in standard from with respect to σ_f, and then apply the template built in Section 5.1.2 to Γ_f.

Continue by applying the template to all columns Γ_s, where f and s have the same parity. That is, for each $t \equiv f \mod 2$ in turn, standardize β with respect to σ_t, and then apply the template designed in Section 5.1.2 to Γ_t. Let B be the resulting branched surface.

In our example, $\mathcal{C}_{\text{odd}} = c_1 + c_3 = 3 + 5 = 8$ and $\mathcal{C}_{\text{even}} = c_2 + c_4 = 2 + 2 = 4$. Thus, we will choose the plumbing arcs in the odd (i.e first and third) Seifert disks; that is, our product disks sit in Γ_1 and Γ_3. We:

1. standardize β with respect to σ_1,
2. apply the template to Γ_1,
3. standardize β with respect to σ_3,

4. apply the template to Γ_3.

We exhibit the result of Steps 1 & 2 in Figure 28 (left), and the result of Steps 3 & 4 in 28 (right). This is the branched surface B for the β in (2.1).

Remark 5.14. *Conjugating the braid does not affect the smoothing directions of the branch locus. That is, the co–orientations on the arcs on F is preserved under braid conjugation.*

5.1.4 Show B is laminar

Our eventual goal is to build taut foliations: we want to build a *laminar* branched surface, apply Theorem 2.4 to get an essential lamination, and finally apply Proposition 3.24 to get a taut foliation. To proceed with this outline, we first verify that B has no sink disks.

Since we built B from a copy of the fiber surface F and a collection of co–oriented product disks, we can classify the branch sectors into three types:

1. the (isotoped) product disks
2. the sectors containing the Seifert disks S_i, or **disk sectors**
3. the remaining sectors, which we call **horizontal sectors**

In Lemma 3.16, we showed that (isotoped) product disks are never sink disks. Therefore, it suffices to show that the disk sectors and the horizontal sectors are sink disks. For our example, we verify this by inspecting Figure 28 (right) directly.

B is sink disk free, so applying Proposition 3.17, we conclude B is a laminar branched surface. Thus, for any $r \in \mathbb{Q}$ carried by the train track τ_B, $S^3_r(K)$ contains an essential lamination $\mathcal{L}_r$: our next goal is to determine the slopes carried by τ_B.

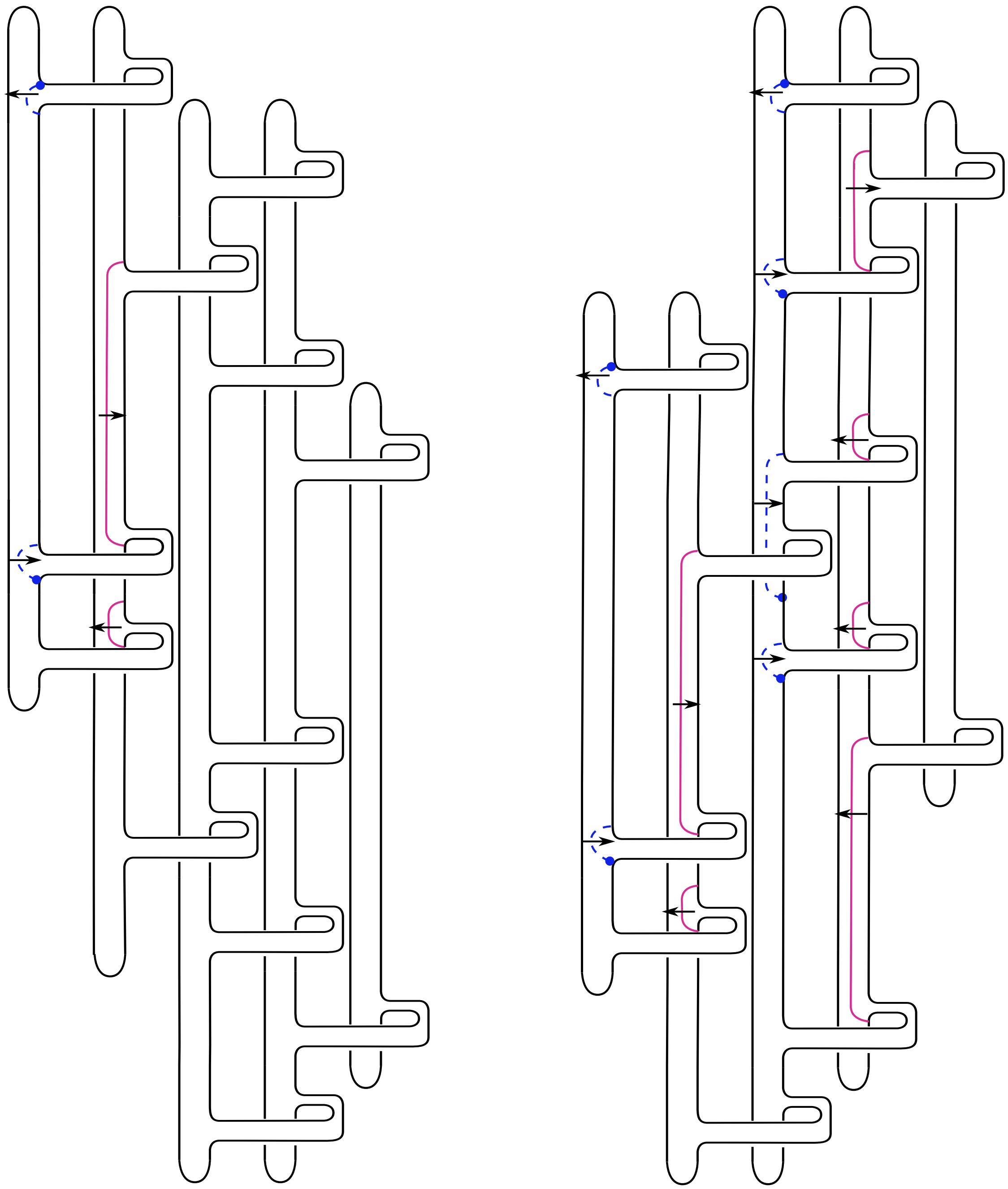

Figure 28: On the left: the braid $\beta = \sigma_1\sigma_3\sigma_2\sigma_3\sigma_4\sigma_1^2\sigma_3\sigma_2\sigma_3\sigma_4\sigma_3$ standardized with respect to σ_1, and the template applied to Γ_1. On the right: we chose a standardization of β with respect to σ_3, and applied the template to Γ_3.

5.1.5 Calculate the slopes carried by τ_B

To compute the slopes carried by τ_B, we first count the total number of product disks used to build B, and then deduct the total number of pairs of linked arcs. We argue that, in fact, our example has no pairs of linked arcs.

Proposition 5.15. *The train track τ_B contains no linked arcs.*

Proof. We chose our product disks to lie in alternating columns. Therefore, the only way to have linked arcs is to have product disks $\mathbb{D}_{\alpha_1}$ and $\mathbb{D}_{\alpha_2}$ in the same column, where:

- the plumbings arcs α_1 and α_2 are consecutive.
- α_1 is cusped to the right, and α_2 is cusped to the left

as in Figure 25. Our template avoids these directions. $\square$

We calculate the slopes carried by τ_B in our example. Here, $\mathcal{C}_{\text{big}} = \mathcal{C}_{\text{odd}} = 8$, so we used $(c_1 - 1) + (c_3 - 1) = \mathcal{C}_{\text{odd}} - 2 = 6$ product disks to build B. Since we have no linked arcs, our train track carries all slopes $r \in (-\infty, 6)$.

Since F is the fiber surface for K,

$$g(K) = g(F) = \frac{\mathcal{C} - n + 1}{2} = \frac{12 - 5 + 1}{2} = 4$$

and τ_B certainly carries all slopes in $(-\infty, g(K))$.

5.1.6 Constructing taut foliations

We are ready to build taut foliations in manifolds obtained by Dehn surgery along $\widehat{\beta}$. First, observe that by section 5.1.4, we have a laminar branched surface B. Second, by Section 5.1.5, the train track τ_B carries all slopes in the interval $(-\infty, g(K))$. Applying Theorem 2.4 yields a family of essential laminations $\mathcal{L}_r$ carried by B, where

$r < g(K)$. Proposition 3.24 extends each essential lamination $\mathcal{L}_r$ to a taut foliation $\mathcal{F}_r$ meeting ∂X_K in simple closed curves of slope r. Performing r-framed Dehn filling produces $S^3_r(K)$ endowed with a taut foliation.

This concludes the example, and the outline of the construction. We emphasize: the key is to understand the distribution of crossings between odd and even columns, and use the more populated set to build the laminar branched surface.

5.2 Proving the positive n–braids theorem

We are almost ready to prove Theorem 5.1. We emphasize: the key aspects of the construction are to build B from a collection of co–oriented product disks such that (1) B is sink disk free, and (2) τ_B carries all slopes in $(-\infty, g(K)-1)$.

5.2.1 Building a sink disk free branched surface

Let β be any positive braid on $n \geq 4$ strands such that $\widehat{\beta}$ is a prime knot. As in Section 5.1.3, compute $\mathcal{C}_{\text{big}}$, and as in Definition 5.13, let Γ_f denote the first column to which we apply the template designed in Section 5.1.2.

We apply our template to all columns Γ_t where $t \equiv f \mod 2$, with one minor modification: if $n-1 \equiv t \mod 2$ (i.e. we include the product disks in last column, Γ_{n-1}, into the branched surface), then we proceed as follows:

- First, standardize β with respect to σ_{n-1} (as in Definition 5.7), except now, do it so that w_1 has a *left* splinter (and not a right splinter).
- If $c_{n-1} = 2$, include no co–oriented plumbing arcs from Γ_{n-1} into B.
- If $c_{n-1} \geq 3$, smooth the first plumbing arc in Γ_{n-1} to the right, and smooth all subsequent plumbing arcs to the left.

Next, we divide positive braids β into two categories, based on the distribution of crossings in the columns used for the construction:

- positive braids where $c_t \geq 3$ for each $t \equiv f \mod 2$ (this is the “generic" case).
- positive braids where $c_t = 2$ for some $t \equiv f \mod 2$ (this is the “edge" case).

This division is necessary: the arguments proving the associated branched surfaces are sink disk free differ; in particular, the second scenario is more nuanced. Nevertheless, both cases have something in common: in Section 5.1.4, we argued that the branch sectors can be split into three types: (1) sectors coming from isotoped product disks, (2) disk sectors, and (3) horizontal sectors. We already know that the first are not sink disks, leaving us to investigate the remaining two types of sectors for both the “generic” and “edge” cases. Showing that we have no disk sectors requires two separate arguments. We show that neither case yields a horizontal sector sink disk in a single Lemma.

Lemma 5.16 (Disk sector analysis for the generic case)**.** *Suppose β is a positive braid such that $c_t \geq 3$ for each $t \equiv f \mod 2$. Then the branched surface B, built as in Section 5.1.3, has no disk sector sink disks.*

Proof. Let Γ_t denote a column whose product disks are used in constructing B. Since $c_t \geq 3$, S_t contains a mix of both left and right smoothed plumbing arcs. So, S_t is not a sink disk. Moreover, this ensures that S_{t+1}, which contains the images of the plumbing arcs, also has a mix of cusp directions. Therefore, if the product disks of Γ_t are included in B, then the disk sectors containing S_t and S_{t+1} are not sink disks. So, we check which columns are utilized to build B, and which are not – the Seifert disks of the former will not be sink disks, and to argue the same for the latter, we do more work. This requires some case analysis.

- If n is odd and $\mathcal{C}_{\text{big}} = \mathcal{C}_{\text{odd}}$, then for every $1 \leq i \leq n-1$, the Seifert disk S_i contains a collection of arcs with both left and right smoothings, so the associated disk sectors are not sink disks. It remains to check that the disk sector containing S_n is not a sink disk, but this is straightforward: the boundary of this disk sector contains all the images of the plumbing arcs from Γ_{n-2}. But since $c_{n-2} \geq 3$, these arcs are smoothed both to the left and to the right. Thus, at least one of these arcs points out of S_n.

- An argument analogous to the one above works for for the case when n is odd and $\mathcal{C}_{\text{big}} = \mathcal{C}_{\text{even}}$: for all $2 \leq i \leq n$, S_i contains a collection of arcs with both left and right smoothings. The disk sector containing S_1 contains all the plumbings arcs in S_2 in the boundary. As $c_2 \geq 3$, we have a mix of smoothing directions in the boundary. In particular, there exists an arc pointing out of the disk sector containing S_1.

- If n is even and $\mathcal{C}_{\text{big}} = \mathcal{C}_{\text{even}}$, then for every $2 \leq i \leq n-1$, the Seifert disks S_i contains a collection of arcs with both left and right smoothings, so the associated disk sectors are not sink disks. Therefore, we need only check that the disk sectors containing S_1 and S_n are not sink disks. Combining the two arguments above yields the desired result.

- If n is even and $\mathcal{C}_{\text{big}} = \mathcal{C}_{\text{odd}}$, then for all $1 \leq i \leq n$, the Seifert disk S_i collection of arcs with both left and right smoothings, so the associated disk sectors are not sink disks.

We deduce that there are no disk sector sink disks. □

Lemma 5.17 (Horizontal sectors for both the generic and edge cases)**.** *Suppose β is a positive braid, and B is the branched surface B built as in Section 5.1.3. B has no horizontal sector sink disks.*

Proof. Fix a horizontal sector $\mathcal{H}$. Consider the portions of $\partial\mathcal{H}$ that are not contained in ∂F: these all come from the branch locus of B. Moreover, scanning the diagram from left–to–right, these alternating between plumbing arcs and images of plumbing arcs. That is, using our coloring conventions for arcs and their images, these portions of $\partial\mathcal{H}$ alternate between blue and pink.

Definition 5.18. *An arc $\alpha \subset F$* ***encloses a band on the left (resp. right)*** *if the left (resp. right) attaching site of a band $\mathbb{b}$ lies in the branch sector $\mathcal{S}$ with $\alpha \subset \partial\mathcal{S}$.*

We observe that every blue arc encloses a band on the left, while every pink arc encloses a band to the right. In particular, this means that when scanning the horizontal sector $\mathcal{H}$ from left–to–right, when we encounter a blue arc α, we can keep moving to the right (the band enclosed by α provides a path to the next Seifert disk).

The right attachment site of $\mathbb{b}$ could be blocked by some image arc, $\varphi(\alpha')$, or it could be unobstructed. In the latter, the horizontal sector $\mathcal{H}$ is in the same branch sector as a Seifert disk; thus, by Lemma 5.16 (and, assuming the forthcoming Lemma 5.16), it is not a sink disk. In the former, the image arc $\varphi(\alpha')$ must be endowed with some co–orientation: if it is smoothed to the left, then $\mathcal{H}$ is not a sink region. If, however, it is smoothed to the right, then our smoothing directions dictate that there must be a right splinter in this sector; see Figure 29. In particular, $\varphi(\alpha')$ encloses a band on the left, and so $\mathcal{H}$ keeps snaking eastwards.

Suppose, by way of contraction, a horizontal sector $\mathcal{H}$ is a sink disk. Thus, every connected component of $\overline{\partial H - \partial F}$ is a right pointing arc, pointing into $\mathcal{H}$. Moreover, the east–most boundary arc must be a pink image arc $\varphi(\alpha'')$. The east–most arc $\varphi(\alpha'')$ lies in the Seifert disk S_j, and either $S_j \neq S_n$ or $S_j = S_n$.

Suppose $S_j \neq S_n$. After conjugating, the east–most portion of $\mathcal{H}$ must look as in Figure 30. In particular, since the east–most arc $\varphi(\alpha'')$ is smoothed to the right, the arc α'' is smoothed to the left. However, our construction prescribes a single left pointing arc in a column $\Gamma_j \neq \Gamma_n$ — in particular, this left–pointer must be

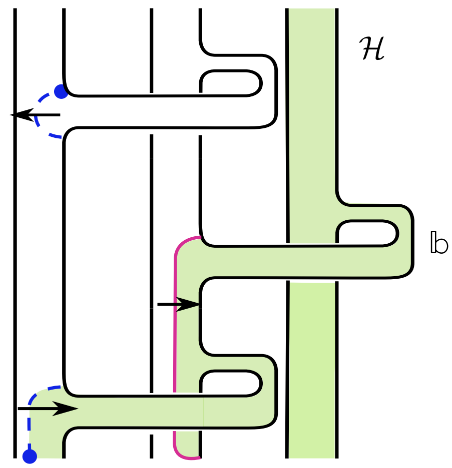

Figure 29: An eastward snaking horizontal sector $\mathcal{H}$, shaded in green. The band $\mathbb{b}$ is a right splinter.

accompanied by a right splinter (as in Figure 29). But this right splinter would be enclosed by $\varphi(\alpha'')$, contradicting that we are at the east–most portion of $\mathcal{H}$. Thus, $S_j = S_n$. See Figure 30.

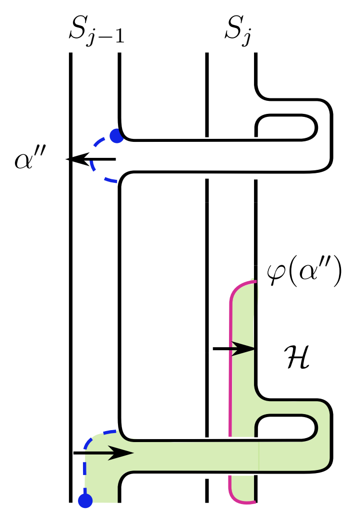

Figure 30: The eastmost boundary of $\mathcal{H}$, shaded in green, cannot lie in S_j with $j < n$. In particular, this local picture does not appear in B (though there could be σ_{j-2} bands between these two σ_{j-1} bands).

Therefore, $\mathcal{H}$ meets S_n. There are two possibilities: either $c_{n-1} = 2$, or $c_{n-1} \geq 3$. If $c_{n-1} = 2$, then we included no co–oriented product disks from Γ_{n-1} into B;

thus, the east–most arc in $\mathcal{H}$ is contained in S_{n-2}, and $\mathcal{H}$ contains Γ_{n-1}; see Figure 31 (left). In particular, this sector is not a **disk**! Thus, it cannot be a sink disk.

Now suppose $\mathcal{H}$ meets S_n, and $c_{n-1} \geq 3$. After conjugating, the east–most portion of $\mathcal{H}$ must look as in Figure 31: note that $\varphi(\alpha'')$ is smoothed to the right, and moreover, there is a (blue) arc α''' preceding it (else $\mathcal{H}$ would be in the same sector as S_{n-1}). Since we are assuming $\mathcal{H}$ is a sink, then α'' must also be smoothed to the right.

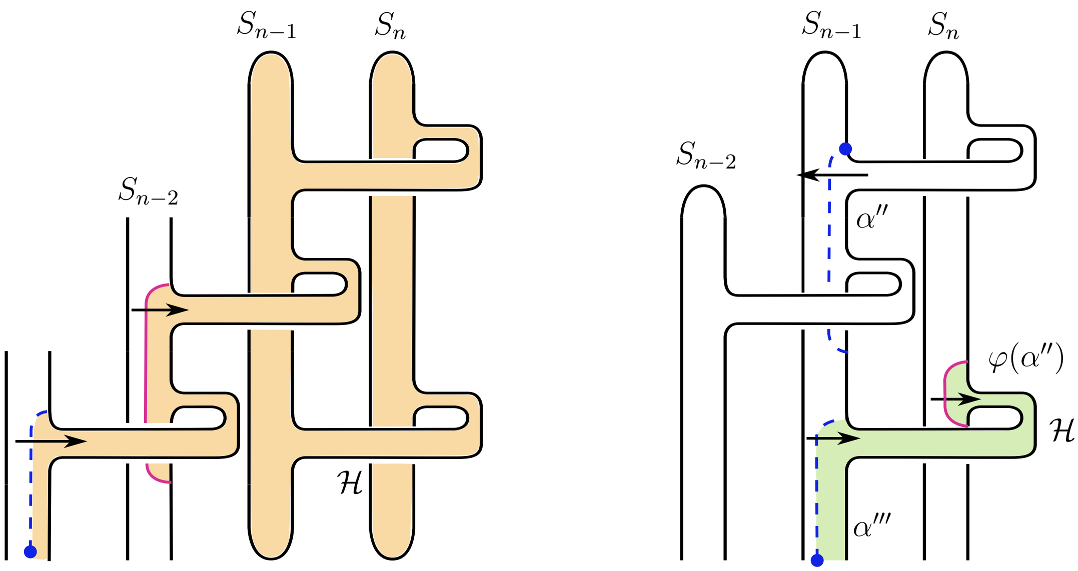

Figure 31: Left: If $c_{n-1} = 2$, the (orange) horizontal sector $\mathcal{H}$ is not a disk. Right: The (green) horizontal sector $\mathcal{H}$ cannot meet S_n in this local model. In particular, this local picture does not appear in B (though there could be σ_{j-2} bands between these two σ_{j-1} bands).

Since $\varphi(\alpha'')$ is smoothed to the right, α'' must be smoothed to the left. However, the cusping directions prescribed by our construction dictate that for plumbing arcs in the last column, all but one of them are left pointing. In particular, looking from top–to–bottom, if left pointing plumbing arc is followed by another plumbing arc, then it must also be left pointing – not right pointing as assumed. We have derived a contradiction.

We conclude that no horizontal sector is a sink disk. $\square$

We now prove the analogous version of Lemma 5.16 for the “edge" case:

Lemma 5.19 (Disk sector analysis for the edge case)**.** *Suppose β is a positive braid where $c_t = 2$ for some $t \equiv f \mod 2$. Then the branched surface B, built as in Section 5.1.3, has no disk sector sink disks.*

Proof. For the columns Γ_m with $c_m \geq 3$, the same argument as in Lemma 5.16 hold. Therefore, we need only consider the Seifert disks S_q with $c_q = 2$, and $q \equiv f \mod 2$. Note that, by our construction, $q \neq n-1$.

Let S_s denote the first Seifert disk with $c_q = 2$, and $q \equiv f \mod 2$ (that is, s is the smallest such q, i.e. the left–most column with this property). Then the disk sector containing S_s is contained in a horizontal sector $\mathcal{H}$ that snakes east–wards; see Figure 32. This is reminiscent of Lemma 5.17; indeed, we will use some of the language and ideas from that proof going forward.

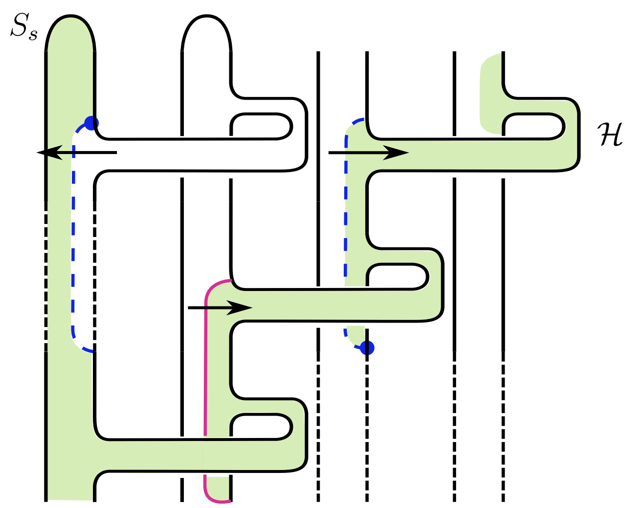

Figure 32: The disk sector containing S_s, where $c_s = 2$, snakes eastwards. It is part of the shaded horizontal sector $\mathcal{H}$, shaded in green. There could be bands with attachment sites in the dashed regions.

Suppose that $\mathcal{H}$ is a sink disk, and every arc in $\overline{\partial\mathcal{H} - \partial F}$ is smoothed to the right. The east–most arc in this set must be an image arc, which we denote $\varphi(\alpha'')$. We claim $\varphi(\alpha'') \subset S_n$.

Suppose, for contradiction, that $\varphi(\alpha'') \subset S_j$ with $j < n$. If we standardize β with respect to σ_j, $\varphi(\alpha'')$ must enclose a band (the right splinter) on the left; see Figure 29. In particular, this band would allow us to move further to the right. But we assumed that $\varphi(\alpha'')$ is the east–most arc, thus arriving at the contradiction.

Therefore, $\mathcal{H}$ is a sink disk which snakes eastward until it meets Γ_n. There are two possibilities: either $c_{n-1} = 2$ or $c_{n-1} \geq 3$ (and there are multiple pink arcs in S_n).

If $c_{n-1} \geq 3$, then $\mathcal{H}$ is in the same branch sector as S_{n-1}; our choices for co–orientations in this case guaranteed this sector contains a mix of smoothing directions. See Figure 33.

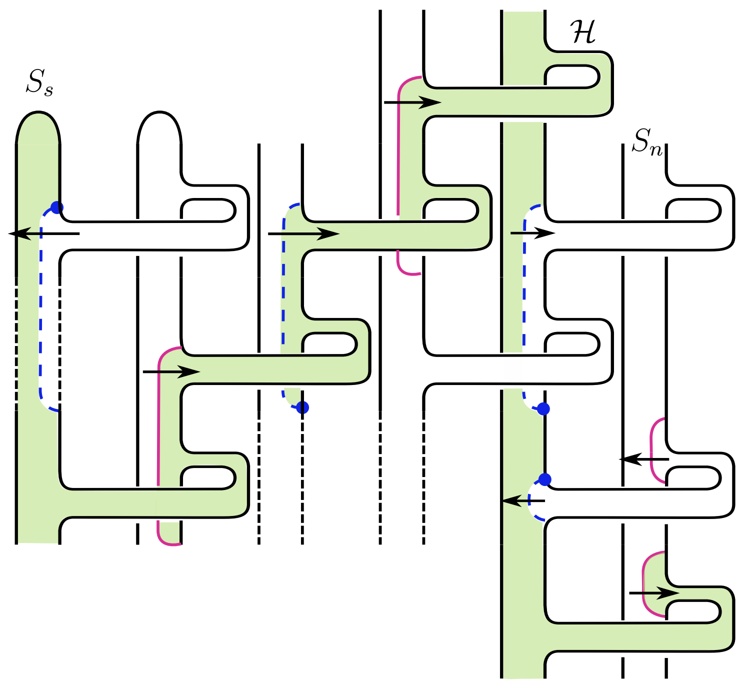

Figure 33: The disk sector containing S_s, where $c_s = 2$, meets S_{n-1}. It is part of the shaded horizontal sector $\mathcal{H}$, shaded in green. There could be bands with attachment sites in the dashed regions. $\mathcal{H}$ is not a sink disk.

If $c_{n-1} = 2$, then H cannot be a sink disk: we did no include any co–oriented product disks from Γ_{n-1}, so the sector containing $\mathcal{H}$ includes S_{n-1} and S_n. In particular,

$b_1(\mathcal{H}) \geq 1$, as in Figure 31 (left).

This concludes our analysis; we deduce that B has no disk sector sink disks. □

Combining the above, we get:

Proposition 5.20. *Applying the construction in Section 5.1.3 to any positive β on $n \geq 4$ strands with $\widehat{\beta}$ a prime knot yields a sink disk free branched surface B.*

Proof. In the generic case, this follows by combining Lemmas 5.16 and 5.17. In the edge case, this follows by combining Lemmas 5.19 and 5.17 □

5.2.2 Understanding the train track τ_B

In our construction, we chose product disks in the more "densely populated" columns. We claim this choice ensures that the train track τ_B carries all slopes $r < g(K)$, where

$$g(K) = \frac{\mathcal{C} - n + 1}{2}$$

Lemma 5.21. *The branched surface B carries all slopes in $(-\infty, g(K) - 1)$.*

Proof. As in Proposition 5.15, our construction almost always guarantees that there are no linked arcs on τ_B – the only exception is when n is even and $\mathcal{C}_{\text{big}} = \mathcal{C}_{\text{odd}}$ with $c_{n-1} \geq 3$; in this case, we have a unique pair of linked arcs.

Therefore, it suffices to count the number of product disks used to build B (and deduct one from the case specified above). The number of product disks used to build B is determined by the parity of the braid index, and the parity of the columns to which we applied our template. We analyze these cases below. Again, we recall: if we use a column Γ_j to build B, then we gain $c_j - 1$ product disks from Γ_j.

- If $n \equiv 1 \mod 2$ and $\mathcal{C}_{\text{big}} = \mathcal{C}_{\text{odd}}$: this means $\mathcal{C}_{\text{odd}} \geq \mathcal{C}/2$, and we are using $(n-1)/2$ columns to build B. Thus we have k unlinked arcs contributing maximally to τ_B, where

$$k = \mathcal{C}_{\text{odd}} - \frac{n-1}{2} \geq \frac{\mathcal{C}}{2} - \frac{n-1}{2} = \frac{\mathcal{C} - n + 1}{2} = g(K)$$

- If $n \equiv 0 \mod 2$ and $\mathcal{C}_{\text{big}} = \mathcal{C}_{\text{even}}$: here, we have $\mathcal{C}_{\text{even}} > \mathcal{C}/2$, and we use $(n/2) - 1$ columns to build B. Therefore, we have k unlinked arcs contributing maximally to τ_B, where

$$\mathcal{C}_{\text{even}} - \left(\frac{n}{2} - 1\right) > \frac{\mathcal{C} - n + 2}{2} > \frac{\mathcal{C} - n + 1}{2} = g(K)$$

- If $n \equiv 1 \mod 2$ and $\mathcal{C}_{\text{big}} = \mathcal{C}_{\text{even}}$: here, we have $\mathcal{C}_{\text{even}} > \mathcal{C}/2$.

  We observe: for $\mathcal{C} - n + 1$ to be divisible by 2, $\mathcal{C}$ must be even. Thus, if $\mathcal{C}_{\text{big}} = \mathcal{C}_{\text{even}}$, we have $\mathcal{C}_{\text{even}} > \mathcal{C}/2$, thus $\mathcal{C}_{\text{even}} \geq \mathcal{C}/2 + 1$.

  We are using $(n-1)/2$ columns to build B. Notice that in this case, we are using product disks in Γ_{n-1} to build B; in particular, when $c_{n-1} \geq 3$, we have a pair of linked arcs. So, we consider two separate cases: (1) $c_{n-1} = 2$ and (2) $c_{n-1} \geq 3$.

  If $c_{n-1} = 2$, then we have k unlinked arcs contributing maximally to τ_B, where

$$k = \mathcal{C}_{\text{even}} - \frac{n-1}{2} - 1 \geq \left(\frac{\mathcal{C}}{2} + 1\right) - \frac{n-1}{2} - 1 = \frac{\mathcal{C} - n + 1}{2} = g(K)$$

  If $c_{n-1} \geq 3$, then we have a single pair of linked arcs in τ_B. So, τ_B contains k unlinked arcs contributing maximally to τ_B, where

$$k = \mathcal{C}_{\text{even}} - \frac{n-1}{2} - 1 > \frac{\mathcal{C} - n + 1}{2} - 1 = g(K) - 1$$

  But notice: τ_B carries all slopes $r \in (-\infty, s)$, where s is an integer. Therefore, if $r \in (-\infty, k)$ and $k > g(K) - 1$, then $k \geq g(K)$, and so we have at least $g(K)$ unlinked arcs in τ_B.

- If $n \equiv 0 \mod 2$ and $\mathcal{C}_{\text{big}} = \mathcal{C}_{\text{odd}}$: as above, we are using co–oriented product disks in Γ_{n-1} to build B. If $c_{n-1} \geq 3$, we have a pair of linked arcs.

  If $c_{n-1} = 2$, then we have no linked arcs in τ_B, so it contains k unlinked arcs contributing maximally to τ_B, with

$$k = \mathcal{C}_{\text{odd}} - \frac{n}{2} - 1 \geq \frac{\mathcal{C} - n}{2} - 1 = g(K) - \frac{3}{2}$$

Since τ_B carries all slopes $r \in (-\infty, s)$, where s is an integer, then we must have that $k \geq g(K) - 1$, and τ_B contains at least $g(K) - 1$ unlinked arcs.

Finally, if $c_{n-1} \geq 3$, then we have a single pair of linked arcs, so τ_B contains k unlinked arcs, where

$$k = \mathcal{C}_{\text{odd}} - \frac{n}{2} - 1 \geq \frac{\mathcal{C} - n}{2} - 1 = g(K) - \frac{3}{2}$$

So $k \geq g(K) - 1$, and we deduce that τ_B carries all slopes $r \in (-\infty, g(K) - 1)$.

We conclude: in all cases, τ_B carries all slopes in $(-\infty, g(K) - 1)$. □

5.2.3 Finishing the proof of Theorem 5.1

Proof of Theorem 5.1. Let β be any positive braid on n–strands such that $\widehat{\beta}$ is a prime knot. By Proposition 5.20, there exists a sink disk free branched surface for B; by Proposition 3.17, it is laminar. By Lemma 5.21, it carries all slopes $r \in (-\infty, g(K) - 1)$. Applying Theorem 2.4 and Proposition 3.24 yields a family of taut foliations $\mathcal{F}_r$ of X_K, meeting ∂X_K in simple closed curves of slope r. Performing r-framed Dehn filling produces $S^3_r(K)$ endowed with a taut foliation. □

Chapter 6

Concluding remarks

6.1 Discussion

To prove Theorem 5.1, we used an arbitrary braid word as it was presented to us. In particular, we mostly utilized conjugation as a way to modify the braid as we built branched surfaces.

Of course, there are other standard ways to modify a braid word and preserve the link type of the closure – by using the relations in the standard Artin presentation of the braid group on n generators. We recall the "close" and "far" relations below:

- The "close" relations: for all $1 \leq i \leq n-2$, $\quad \sigma_i \; \sigma_{i+1} \; \sigma_i = \sigma_{i+1} \; \sigma_i \; \sigma_{i+1}$
- The "far" relations: for all $|i-j| \geq 2$, $\quad \sigma_i \; \sigma_j = \sigma_j \; \sigma_i$.

We never applied these braid relations while constructing B! Moreover, we make the following observation: fix a braid word β, and compute $\mathcal{C}_{\text{odd}}$ and $\mathcal{C}_{\text{even}}$ as in Chapter 5. If we could apply a "close" relation to β to produce a "braid synonym" β', the values of $\mathcal{C}_{\text{odd}}$ and $\mathcal{C}_{\text{even}}$ will change (one will increase by one, the other will decrease by one, depending on the parity of i). Thus, if we had a braid β where we could apply the "close" relations many times, we could drastically change the distribution of crossings between the odd and even columns of β. This suggests a natural question:

Question 6.1. *Fix β be a positive n–braid, and let*

$$\mathcal{C}_{\mathit{diff}}(\beta) := \max\{\ |\mathcal{C}_{odd}(\beta') - \mathcal{C}_{even}(\beta')|\ \}$$

where we maximize over all possible synonyms β' of β. How big can $\mathcal{C}_{\mathit{diff}}(\beta)$ get for a fixed isotopy class of the braid closure?

If one could always make $\mathcal{C}_{\text{diff}}(\beta)$ (much) bigger than $g(K)$, then in fact, the proof of Theorem 5.1 produces taut foliations in $S^3_r(K)$, where $r \in (\infty, m)$, where $2g(K) - 1 > m >> g(K)$. Using the braid relations to "imbalance" a braid (i.e. force as many crossings as possible into either the odd or even columns) is a strategy used by Baader–Feller–Lewark–Zentner [BFLZ19] and Feller [Fel16] to investigate the dealternation numbers and signatures of positive braids, respectively. One may hope: if we could

1. answer Question 6.1, and
2. build B using a co–oriented product disk for every plumbing arc,

then perhaps we could prove:

for any positive braid with closure a prime knot, and any $r \in (-\infty, 2g(K) - 1)$, $S^3_r(K)$ has a taut foliation.

Of course, at this time, this is merely speculation, as there are combinatorial challenges with arguing that the branched surface is sink disk free, and that the train track τ_B carries all slopes $r < 2g(K) - 1$.

Murasugi famously classified all 3–braids up to conjugation [Mur74]; no such classification exists for higher braid index. We suspect: the difficulty in generalizing Theorem 1.15 to the statement above reflects this missing classification.

6.2 Future directions

In this section, we present some potential directions for future projects. Pursuing them would require building on the techniques developed here, while developing some new strategies, too.

Problem 6.2. *Show that for any positive braid β with $\widehat{\beta} \approx K$ a prime knot, $S^3_r(K)$ has a taut foliation for every $r \in (-\infty, 2g(K)-1)$, .*

Problem 6.3. *Show that for any fibered knot K with right–veering monodromy and $r \in (-\infty, g(K))$, $S^3_r(K)$ has a taut foliation.*

Problem 6.4. *Show that for any (hyperbolic) fibered knot K of genus $g \geq 2$ and $r \in (-\infty, 2)$, $S^3_r(K)$ has a taut foliation.*

Bibliography

[Baa13] Sebastian Baader, *Positive braids of maximal signature*, Enseign. Math. **59** (2013), no. 3-4, 351–358. MR 3189041

[BFLZ19] Sebastian Baader, Peter Feller, Lukas Lewark, and Raphael Zentner, *Khovanov width and dealternation number of positive braid links*, Math. Res. Lett. **26** (2019), no. 3, 627–641. MR 4028096

[BM18] Kenneth L. Baker and Allison H. Moore, *Montesinos knots, Hopf plumbings, and L-space surgeries*, J. Math. Soc. Japan **70** (2018), no. 1, 95–110. MR 3750269

[Ber18] John Berge, *Some knots with surgeries yielding lens spaces*, https://arxiv.org/abs/1802.09722 (2018).

[Bow16] Jonathan Bowden, *Approximating C^0-foliations by contact structures*, Geom. Funct. Anal. **26** (2016), no. 5, 1255–1296.

[BC15] Steven Boyer and Adam Clay, *Slope detection, foliations in graph manifolds, and L-spaces*, https://arxiv.org/abs/1510.02378 (2015).

[BC17] Steven Boyer and Adam Clay, *Foliations, orders, representations, L-spaces and graph manifolds*, Adv. Math. **310** (2017), 159–234.

[BGW13] Steven Boyer, Cameron McA. Gordon, and Liam Watson, *On L-spaces and left-orderable fundamental groups*, Math. Ann. **356** (2013), no. 4, 1213–1245.

[BNR97] Mark Brittenham, Ramin Naimi, and Rachel Roberts, *Graph manifolds and taut foliations*, J. Differential Geom. **45** (1997), no. 3, 446–470.

[CLW13] Adam Clay, Tye Lidman, and Liam Watson, *Graph manifolds, left-orderability and amalgamation*, Algebr. Geom. Topol. **13** (2013), no. 4, 2347–2368.

[Deh10] M. Dehn, *Über die Topologie des dreidimensionalen Raumes*, Math. Ann. **69** (1910), no. 1, 137–168. MR 1511580

[DRa] Charles Delman and Rachel Roberts, *Persistently foliar composite knots*, https://arxiv.org/abs/1905.04838.

[DRb] Charles Delman and Rachel Roberts, *Personal communication.*

[EHN81] David Eisenbud, Ulrich Hirsch, and Walter Neumann, *Transverse foliations of Seifert bundles and self-homeomorphism of the circle*, Comment. Math. Helv. **56** (1981), no. 4, 638–660.

[Fel16] Peter Feller, *Optimal cobordisms between torus knots*, Comm. Anal. Geom. **24** (2016), no. 5, 993–1025. MR 3622312

[FS80] Ronald Fintushel and Ronald J. Stern, *Constructing lens spaces by surgery on knots*, Math. Z. **175** (1980), no. 1, 33–51.

[FO84] W. Floyd and U. Oertel, *Incompressible surfaces via branched surfaces*, Topology **23** (1984), no. 1, 117–125.

[Gab83] David Gabai, *Foliations and the topology of* 3*-manifolds*, J. Differential Geom. **18** (1983), no. 3, 445–503.

[Gab85] ______, *The Murasugi sum is a natural geometric operation. II*, Combinatorial methods in topology and algebraic geometry (Rochester, N.Y., 1982), Contemp. Math., vol. 44, Amer. Math. Soc., Providence, RI, 1985, pp. 93–100.

[Gab86] ______, *Detecting fibred links in S^3*, Comment. Math. Helv. **61** (1986), no. 4, 519–555.

[Gab87] ______, *Foliations and the topology of 3-manifolds. III*, J. Differential Geom. **26** (1987), no. 3, 479–536.

[Gab90] ______, *1-bridge braids in solid tori*, Topology Appl. **37** (1990), no. 3, 221–235.

[GO89] David Gabai and Ulrich Oertel, *Essential laminations in 3-manifolds*, Ann. of Math. (2) **130** (1989), no. 1, 41–73.

[Ghi08] Paolo Ghiggini, *Knot Floer homology detects genus-one fibred knots*, Amer. J. Math. **130** (2008), no. 5, 1151–1169. MR 2450204

[GL89] C. McA. Gordon and J. Luecke, *Knots are determined by their complements*, J. Amer. Math. Soc. **2** (1989), no. 2, 371–415. MR 965210

[GLV18] Joshua Evan Greene, Sam Lewallen, and Faramarz Vafaee, $(1,1)$ *L-space knots*, Compos. Math. **154** (2018), no. 5, 918–933.

[HRRW15] Jonathan Hanselman, Jacob Rasmussen, Sarah Dean Rasmussen, and Liam Watson, *Taut foliations on graph manifolds*, https://arxiv.org/abs/1508.05911 (2015).

[Hed10] Matthew Hedden, *Notions of positivity and the Ozsváth-Szabó concordance invariant*, J. Knot Theory Ramifications **19** (2010), no. 5, 617–629. MR 2646650

[HKM07] Ko Honda, William H. Kazez, and Gordana Matić, *Right-veering diffeomorphisms of compact surfaces with boundary*, Invent. Math. **169** (2007), no. 2, 427–449. MR 2318562

[Juh15] András Juhász, *A survey of Heegaard Floer homology*, New ideas in low dimensional topology, Ser. Knots Everything, vol. 56, World Sci. Publ., Hackensack, NJ, 2015, pp. 237–296.

[KR13] William H. Kazez and Rachel Roberts, *Fractional Dehn twists in knot theory and contact topology*, Algebr. Geom. Topol. **13** (2013), no. 6, 3603–3637. MR 3248742

[KR17] ______, *C^0 approximations of foliations*, Geom. Topol. **21** (2017), no. 6, 3601–3657.

[KMOS07] P. Kronheimer, T. Mrowka, P. Ozsváth, and Z. Szabó, *Monopoles and lens space surgeries*, Ann. of Math. (2) **165** (2007), no. 2, 457–546.

[LV19] Cristine Lee and Faramarz Vafaee, *On 3-braids and L-space knots*, https://arxiv.org/abs/1911.01289 (2019).

[Li02] Tao Li, *Laminar branched surfaces in 3-manifolds*, Geom. Topol. **6** (2002), 153–194.

[Li03] ______, *Boundary train tracks of laminar branched surfaces*, Topology and geometry of manifolds (Athens, GA, 2001), Proc. Sympos. Pure Math., vol. 71, Amer. Math. Soc., Providence, RI, 2003, pp. 269–285.

[Lic62] W. B. R. Lickorish, *A representation of orientable combinatorial 3-manifolds*, Ann. of Math. (2) **76** (1962), 531–540. MR 151948

[LM16] Tye Lidman and Allison H. Moore, *Pretzel knots with L-space surgeries*, Michigan Math. J. **65** (2016), no. 1, 105–130.

[LS09] Paolo Lisca and András I. Stipsicz, *On the existence of tight contact structures on Seifert fibered 3-manifolds*, Duke Math. J. **148** (2009), no. 2, 175–209.

[Liv04] Charles Livingston, *Computations of the Ozsváth-Szabó knot concordance invariant*, Geom. Topol. **8** (2004), 735–742. MR 2057779

[Mos71] Louise Moser, *Elementary surgery along a torus knot*, Pacific J. Math. **38** (1971), 737–745.

[Mur74] Kunio Murasugi, *On closed* 3*-braids*, American Mathematical Society, Providence, R.I., 1974, Memoirs of the American Mathmatical Society, No. 151. MR 0356023

[Ni07] Yi Ni, *Knot Floer homology detects fibred knots*, Invent. Math. **170** (2007), no. 3, 577–608.

[Nie19] Zipei Nie, *Left-orderablity for surgeries on* $(-2, 3, 2s + 1)$*-pretzel knots*, Topology Appl. **261** (2019), 1–6. MR 3946327

[Nov65] S. P. Novikov, *The topology of foliations*, Trudy Moskov. Mat. Obšč. **14** (1965), 248–278. MR 0200938

[OS04] Peter Ozsváth and Zoltán Szabó, *Holomorphic disks and genus bounds*, Geom. Topol. **8** (2004), 311–334.

[OS05] ______, *On knot Floer homology and lens space surgeries*, Topology **44** (2005), no. 6, 1281–1300.

[RR17] Jacob Rasmussen and Sarah Dean Rasmussen, *Floer simple manifolds and L-space intervals*, Adv. Math. **322** (2017), 738–805.

[Ree52] Georges Reeb, *Sur certaines propriétés topologiques des variétés feuilletées*, Actualités Sci. Ind., no. 1183, Hermann & Cie., Paris, 1952, Publ. Inst. Math. Univ. Strasbourg 11, pp. 5–89, 155–156. MR 0055692

[RSS03] R. Roberts, J. Shareshian, and M. Stein, *Infinitely many hyperbolic 3-manifolds which contain no Reebless foliation*, J. Amer. Math. Soc. **16** (2003), no. 3, 639–679. MR 1969207

[Rob01a] Rachel Roberts, *Taut foliations in punctured surface bundles. I*, Proc. London Math. Soc. (3) **82** (2001), no. 3, 747–768.

[Rob01b] ———, *Taut foliations in punctured surface bundles. II*, Proc. London Math. Soc. (3) **83** (2001), no. 2, 443–471.

[Rud93] Lee Rudolph, *Quasipositivity as an obstruction to sliceness*, Bull. Amer. Math. Soc. (N.S.) **29** (1993), no. 1, 51–59.

[Sta78] John R. Stallings, *Constructions of fibred knots and links*, Algebraic and geometric topology (Proc. Sympos. Pure Math., Stanford Univ., Stanford, Calif., 1976), Part 2, Proc. Sympos. Pure Math., XXXII, Amer. Math. Soc., Providence, R.I., 1978, pp. 55–60.

[Thu97] William P. Thurston, *Three-dimensional geometry and topology. Vol. 1*, Princeton Mathematical Series, vol. 35, Princeton University Press, Princeton, NJ, 1997, Edited by Silvio Levy. MR 1435975

[Tra19] Anh Tuan Tran, *Left-orderability for surgeries on twisted torus knots*, Proc. Japan Acad. Ser. A Math. Sci. **95** (2019), no. 1, 6–10. MR 3896142

[Vaf15] Faramarz Vafaee, *On the knot Floer homology of twisted torus knots*, Int. Math. Res. Not. IMRN (2015), no. 15, 6516–6537.

[Wal60] Andrew H. Wallace, *Modifications and cobounding manifolds*, Canadian J. Math. **12** (1960), 503–528. MR 125588